4-2019

Utilizing Geophysical Attributes to Investigate the Architecture of a Pinnacle Reef Complex, Michigan Basin, USA

Austin M. Johnson
Western Michigan University

Follow this and additional works at: https://scholarworks.wmich.edu/masters_theses

Part of the Geology Commons

Recommended Citation

UTILIZING GEOPHYSICAL ATTRIBUTES TO INVESTIGATE THE ARCHITECTURE OF A
PINNACLE REEF COMPLEX, MICHIGAN BASIN, USA

by

Austin M. Johnson

A thesis submitted to the Graduate College
in partial fulfillment of the requirements for
the degree of Master of Science
Geosciences
Western Michigan University
April 2019

Thesis Committee:

Michelle Kominz, Ph.D.
William Harrison III, Ph.D.
William Sauck, Ph.D.

ACKNOWLEDGEMENTS

UTILIZING GEOPHYSICAL ATTRIBUTES TO INVESTIGATE THE ARCHITECTURE OF A
PINNACLE REEF COMPLEX, MICHIGAN BASIN, USA

Austin M. Johnson, M.S.

Western Michigan University, 2019

The Silurian Niagaran Pinnacle Reefs of the Michigan Basin retain their relevance after primary recovery of hydrocarbons and are excellent candidates for carbon dioxide sequestration, natural gas storage, and enhanced oil recovery. Due to the nature of carbonate rocks, these reef complexes are heterogeneous and lateral interpolation between observations in wells, is ambiguous. Ambiguity has led to large uncertainty and disagreement regarding reef architectures and their internal facies distributions. Previous models of these reef complexes have relied almost entirely on well logs and conventional core. This study focused on integrating 3D seismic reflection data to reduce uncertainty when delineating the overall shape of the Charlton 30-31 reef complex. For this study, seismic attributes extracted from the 3D seismic data were pivotal when investigating the on-reef and off-reef characteristic of the 3D seismic data. The Charlton 30-31 reef complex displayed an asymmetrical overall architecture, with discontinuous seismic signatures within the reef interior. However, the internal facies of the reef were determined to be under the detection limit of the seismic data. This study demonstrates the value of 3D seismic data and seismic attributes when investigating the overall architecture of a reef complex without abundant well control.

TABLE OF CONTENTS

Table of Contents-Continued

LIST OF TABLES

LIST OF FIGURES

List of Figures-Continued

LIST OF PLATES

CHAPTER I

INTRODUCTION

Purpose of Investigation

The Silurian Niagaran pinnacle reefs of the Michigan Basin have been heavily studied

since their initial discovery in the 1960's. A Silurian pinnacle reef in this study, is an isolated

biohermal structure of Silurian age. These structures are made up of carbonate rocks, have

roughly the shape of a dome, and are generally less than two miles long (Bristol, 1974). The

exceptional interest in Pinnacle Reefs stems from their tendency to host immense amounts of

hydrocarbons. Pinnacle Reef reservoirs in the Michigan Basin are responsible for a significant

amount of the oil and gas production in Michigan, having produced over 500 million barrels of

oil and 2.9 trillion cubic feet of natural gas (Rine, 2015). Although these fields are nearing the

end of their primary production they retain their relevance due to the significant amount of

original oil still in place and their potential for storing carbon dioxide and natural gas (Grammer

et al., 2008; Toelle et al., 2008). In fact, carbon dioxide sequestration, natural gas storage, and

Enhanced Oil Recovery (EOR) have been accomplished in a few of these fields (Toelle et al.,

2008). Numerous studies have developed static geologic models to better understand the

complexity of Pinnacle Reef architectures (e.g. Gill, 1973; Huh, 1973; Mesolella et al., 1974;

Rine, 2015). These studies were based primarily on petrophysical data. One disadvantage of

using petrophysical data is the limited spatial scale of the data. That is, a well represents a

single data point in space. If petrophysical data can be coupled with geophysical data, the void between data points may be eliminated, generating a continuous geological data set.

This study focused on bridging geology and geophysics to better understand the internal and off-reef architecture of the Charlton 30-31 Pinnacle Reef, located in Otsego County, Michigan (Figure 1). The precise architecture of the Charlton 30-31 Pinnacle Reef was not previously described, as prior studies investigated only the reservoir (Toelle, 2012). Primary hydrocarbon production for the Charlton 30-31 field began in 1974. Primary production had ceased, and the field was abandoned in 1997. Following its abandonment, in 2004 intentions to develop the field for CO_2 EOR led to the acquisition of a 3D seismic survey that encompassed the entire field. The 3D seismic survey shot in 2004 serves as a "Baseline" survey. A "Baseline" survey precedes a "Monitor" survey, acquired subsequently to observe dynamic changes in the subsurface due to injection of CO_2 during EOR. In this case, a "Monitor" survey was shot in 2007, following the commencement of CO_2 flooding of the reef in 2005. In addition to the "Baseline" and "Monitor" surveys, data within the survey boundaries includes 12 wells with a suite of logs. This study qualitatively compared published static geological models for Pinnacle Reefs, with the seismic signature of the Charlton 30-31 reef complex in northern Michigan. The hypothesis of this study is that the observed architecture of the Charlton 30-31 reef complex reflects the model proposed by (Rine, 2015). The objectives of this study are to: (i) develop a work flow for coupling petrophysics and geophysics to define internal reef architectures, (ii) understand the detection limit of the high-resolution 3D seismic data for this study, and (iii) establish the geometry of the reef complex.

<u>Fundamental Questions</u>

- *Is the seismic data resolution fine enough to detect internal reef architectures within the seismic survey utilized in this study?*

- *Do either of the published static geologic models reflect the reef geometry observed in the 3D seismic survey?*

- *What are the characteristics of the off-reef seismic signatures in this seismic survey?*

Background

<u>Geologic Setting</u>

The Michigan Basin is a circular, intracratonic depression that encompasses much of Michigan's Lower Peninsula, as well as portions of the Upper Peninsula and of adjacent states. The Silurian-aged reefs occur in the upper Niagaran Guelph Formation (Brown Niagaran), within the Michigan Basin and can be found in two distinct trends (see Figure 1). The linear trending reef belts line the northern and southern basin margins and are presently buried at depths of 3000-7000 feet (915-2135 meters) (Toelle, 2012). The reefs average 350 feet (107 meters) in height, with some reaching up to 700 feet (210 meters) (Toelle, 2012). The northern trend hosts taller, slightly slenderer reefs with steeper sloping flanks. In the southern trend the reefs are typically shorter, with broader sloping reef geometries. These Pinnacle Reef reservoirs are primarily composed of carbonate but do display some variation in mineralogy. The reservoirs can vary in composition, from entirely limestone with some partially dolomitized reservoirs, to completely dolomitized. The Charlton 30-31 reef is in the northern reef trend and, as such, is relatively tall with steep sloping flanks. This reef covers an aerial extent of roughly 0.5 square

3

miles (1.2 square kilometers). The stacking pattern of contemporaneous formations in the

Michigan Basin is well known for off-reef strata. During the Silurian multiple sea-level

regressions and transgressions resulted in alternating evaporite and carbonate beds (Figure 2).

Previous Work

A previous study developed a workflow for recognizing carbonate buildups in 3D seismic

data (Bubb and Hatlelid, 1978). They describe the necessary steps to properly identify

carbonate buildups with several examples from around the world. To directly define the

boundary of the carbonate buildup in the seismic profile, significant depositional topography is

necessary. Indirect criteria for recognizing the buildups include drape, velocity anomalies, and

spurious events (Figure 3). Drape is common where overlying stratigraphy envelope the

carbonate buildup expressing relief. The effects of drape tend to decrease stratigraphically

upward (Fig 3: II-A1). Velocity anomalies are common indicators because significant seismic

velocity contrast generally exists between the carbonate buildup and adjacent evaporites. For

example, strata underlying the buildup with higher velocity properties than laterally adjacent

strata will be "pulled-up" in time (Fig 3: II-A2). Spurious events are odd events that occur at the

edges of buildups. The edges of buildups are commonly marked by termination of surrounding

beds against the buildup. The authors warn that these indicators are not unique to carbonate

buildups and can also result from salt intrusions, igneous intrusions, and other geological

structures. To avoid incorrectly identifying these other structures as carbonate buildups in the

seismic profile, the interpreter must consider all available regional geologic and geophysical

data.

A study done by Kleipool et al. (2017) demonstrated a method of integrating petrophysical and geophysical data. The authors conducted their study on a package of heterogeneous carbonate rocks in Las Negras, Spain. They began by analyzing the petrophysical data and were able to identify several facies. Synthetic seismic profiles were created from the petrophysical data and when convolved with high-frequency wavelets, the synthetic seismograms had major reflectors coinciding with: sequence boundaries, diagenetic zones, and a boundary between the basement and the overlying carbonates. They were able to confirm this because the study was performed on a package of rock that outcropped. The modeling methods utilized for integrating the petrophysical data and geophysical data from Kleipool et al. (2017) were considered for this study. The author's modeling methods included: geological modeling, rock properties modeling, and synthetic seismogram modeling. Synthetic seismogram modeling and comparison with well logs is critical for identifying subtle signatures in a seismic profile.

Gill (1973) reconstructed the architecture and depositional history of the pinnacle reefs in the Michigan Basin. Gill utilized wire-line logs, core lithologies, and core analysis data from 54 wells that were all located within a single field or in close proximity to that field. That is, a suite of wells penetrated the reef, reef-flank, and off-reef locations. Core descriptions were prepared from slabbed core observations, petrography, core analysis data and petrophysical logs. This abundance of data was used to construct a geologic model. Where there were data voids between wells, Gill's model extrapolated the data from well to well based on observations of the data and geologic principles. The model developed based on Gill's study proposed that the

reef complexes are approximately symmetrical in shape with an unpredictable internal facies

distribution (Figure 4).

Rine (2015) developed a different facies architecture model for the Silurian Niagaran

reef complexes in the Michigan Basin. Rine utilized multiple reef complexes but primarily

focused on one specific reef due to the wealth of core (20 cores) in its field. Core description

was carried out using a hand lens and a microscope, as well as core analysis data. Gamma-ray

(GR) logs were coupled with the core descriptions to derive GR signatures unique to the reef

facies. Facies distributions were mapped in wells that lacked core by using their GR signatures.

A highly asymmetric reef geometry with relatively well-defined internal facies distributions was

developed. Rine (2015) suggested that the paleowind direction during the time of deposition

influenced the facies distribution and the overall reef geometry (Figure 5).

The Charlton 30-31 reef complex was studied by Toelle (2012) to better understand its

reservoir quality. Extensive reservoir characterization was performed utilizing wireline log data,

production data, and the "Baseline" 3D seismic survey acquired prior to the CO_2 flooding of the

reef. Toelle's (2012) study was undertaken to strategically place injection wells in the reef and

to target high flow zones, maximizing tertiary oil recovery. Toelle's investigation suggested that

zones of attenuation of high frequency seismic waves in the reservoir correspond to high

porosity/permeability zones that were drained of hydrocarbons. The second portion of Toelle's

study utilized static rock characteristics to develop a dynamic forward model to simulate the

migration path of the injected CO_2. This study was tested with production data, obtained from

two new wells drilled subsequent to the "Baseline" study. Additionally, the 3D seismic

"Monitor" survey acquired following the study was used to test the model. The results of the

"Monitor" survey were consistent with the theory that attenuation of high frequency seismic signals can be an indicator of high porosity, high permeability zones within the reservoir.

Data Description

This study utilized a variety of both geophysical and petrophysical data to determine the rock characteristics of the Charlton 30-31 field. The Charlton 30-31 field was discovered in 1972 when the Salling Hanson #1-31 well (PN: 29073) was drilled in the southern part of the field. Sonic (SON), gamma-ray (GR), and bulk density (RHOB) logs were run for this well. These logs were considered standard at that time. Following the discovery of the field, 6 new wells were drilled that penetrated the reef. Again, multiple logs were acquired for these wells. All the wells utilized in this study were drilled vertically with the exception of the State Charlton "C" 2-30 well (PN: 30203), drilled in 1975. The State Charlton "C" 2-30 was drilled deviated so the borehole entered the reef northwest of its surface location. This study utilized an additional 5 wells drilled in off-reef locations but within the area of the seismic survey. In total, 12 wells and their respective well logs within the 3D seismic survey boundary for the Charlton 30-31 field were utilized for the petrophysical component of this study (Figure 6). This study used GR, RHOB, neutron porosity (NPHI), and SON logs for geologic interpretation (Table 1). Due to the lack of a core at the depth of investigation in the Charlton 30-31 field, a core and its respective well logs from an analog well were used to improve the accuracy of well log interpretations for the Charlton 30-31 field. The Charlton 4 field served as the analog field for this study due to its proximity, its Brown Niagaran lithology, and the core with logs available from within the reef complex (Figure 7). One 3D seismic survey loaned by Core Energy, provided the geophysical data used in this study. This survey was acquired by Bay Geophysical in September of 2007 and

covered an area of 2.5 square miles (6.5 square kilometers). The areal bin dimension was 82.5

by 82.5 feet (25 by 25 meters). During acquisition, dynamite was used to supply the acoustic

energy source and the resulting processed volume had a sample rate of 1 millisecond.

Following acquisition, the raw seismic data was processed by two companies, WesternGeco and

Sterling Seismic. Utilizing two companies improves the chances that any data artifacts derived

from the processing sequence will be accounted for and resolved during interpretation.

CHAPTER II

METHODS

Petrophysical

Gamma-Ray Log

The GR log was pivotal for the initial phase of identifying and interpreting facies in non-

cored wells for this study. The GR log measures the total natural gamma ray radiation from

uranium, potassium, and thorium in a rock. These elements are dominantly associated with

siliciclastic sediments and are often used as indicators for depositional environments (i.e. facies

change from deep marine muds to shallow detrital sands). Because this study does not involve

siliciclastic sediments and concentrates on carbonate (typically low GR signatures) and

evaporate deposits, the scale of the GR log was displayed on an amplified scale of 0 to 50

American Petroleum Institute (API) units (conventional display is 0 to 150) (Rine, 2015). This

improves identification of lower amplitude spikes in the GR signature. Facies changes were

interpreted from the GR signatures throughout the log. In the initial interpretation phase,

common GR signatures found in the reef complexes analyzed by Rine (2015), were used to help interpret the 12 wells within the area of interest. An additional well (PN: 28006) from the Charlton 4 field served as an analog well and was interpreted utilizing the same approach. The Charlton 4 field is in close proximity and the Brown Niagaran is dominantly dolomitized in both the Charlton 30-31 field and the Charlton 4 field. The 28006 well was selected from the Charlton 4 field because the well was cored through the entirety of the reef and multiple down-hole logs were collected (GR, SON, NPHI, & RHOB).

Core Description

To provide a measure of the accuracy of the initial GR interpretations, a second method of facies identification was utilized to interpret the analog well. The core material from the 28006 well was analyzed using a hand-lens and dilute (10%) hydrochloric acid (HCl). Characteristics that were recorded include lithology, fossil content, sedimentary structures, and stratigraphic surfaces. These two analytical techniques were coupled with the geophysical logs to produce a detailed core description. The facies identified in the core description were compared to the facies generated using Rine (2015) interpretations, based on GR. A limitation to this method is that depths associated with the core do not always correspond exactly with the depths derived from wireline logs. Rine's method utilizing GR log signatures and core description depths, were utilized to improve the correlation between the core and log depths. The improved GR interpretations for the analog field were used to refine the Charlton 30-31 GR log generated facies interpretations.

Geologic Model

In Schlumberger software module Petrel, the facies interpretations for the 12 wells within the 3D seismic survey were utilized to develop two geologic models for the Charlton 30-31 field. A southwest to northeast transect incorporating 5 wells, the respective logs, and the surface elevation tops (well tops), was used to generate a 2D cross-section through the study area (Figure 8). The cross-section was drawn to capture the variability across the reef complex and best represent the Charlton 30-31 field. The cross-section was exported from Petrel and became the groundwork for the geologic models developed in Adobe Illustrator. The advantage of free hand modeling in Illustrator is the operator's ability to define the resolution and extrapolation manner for the model. A well serves as a single data point in the spatial grid, thus there is only data where there are wells. The depositional facies and formations must be extrapolated where petrophysical data does not exist. This is critical in this study because two extrapolation techniques were utilized to determine which technique yields a geologic model most consistent with the seismic survey observations. An example of the two extrapolation techniques is shown in figure 9, resembling models and interpretations made by Gill and Rine of the Belle River Mills reef (modified from Rine et al. 2017). The first model developed utilizes Gill's model of the pinnacle reefs. Gill (1973) proposed that the pinnacle reefs in Michigan have a symmetrical architecture with unpredictable, vertical and lateral distribution of reef facies (Figure 9-I). The second geologic model was developed utilizing Rine's (2015) approach to modeling Michigan pinnacle reefs. Rine proposed that the pinnacle reefs are asymmetrical with a predictable distribution of reef facies. That is, Rine's geologic model suggests that the reefs are comprised of a windward, steep sloping flank and a leeward, gently sloping flank with

predictable windward and leeward facies (Figure 9-II). When developing the geologic model for the Charlton 30-31 reef using this approach the facies were extrapolated between wells based on the prevailing winds.

<u>Well-to-Seismic Cross Section Tie</u>

The first step in executing a well-to-seismic section tie, is generating a synthetic seismogram for the well. To generate synthetic seismograms for the wells, it is mandatory to calculate the acoustic impedances at every significant lithology change in each well. Acoustic impedance (the product of sonic velocity and bulk density) is computed for a well using the respective SON and RHOB logs. Either the SON or the RHOB logs were available for many of the wells within the reef complex as well as in the off-reef rocks (Table 1) while only one well (PN: 29073) had both SON and RHOB logs. To generate multiple well-to-seismic ties, RHOB logs were created using Gardner's equation (Gardner et al., 1974). Gardner's equation is derived from an empirical relationship between density (ρ) and velocity (v) of the more prevalent sedimentary rock types (Figure 10). Mathematically it is represented by the equation:

$$\rho = 0.23v^{.25} \qquad \text{(Equation 1)}$$

To validate the method, a pseudo RHOB log was generated using Gardner's equation for the 29073 well because RHOB and SON logs were available for this well. The two were then semi-quantitatively compared (Figure 11). After confirming the validity of the Gardner's (1974) method, pseudo RHOB logs were generated for wells with: SON logs present and RHOB logs absent. The next step after obtaining the necessary logs was multiplying the SON log by the RHOB log of each well to yield that well's acoustic impedance. Acoustic impedance contrasts govern seismic reflection coefficients at an interface between two media (Gardner et al., 1974).

The acoustic impedance calculations for each well were used to compute the reflection

coefficients. The equation for reflection coefficients is:

$$R = (\rho_2 V_2 - \rho_1 V_1) / (\rho_2 V_2 + \rho_1 V_1) \qquad \text{(Equation 2)}$$

The next step was extracting a wavelet using the Roy White Extended algorithm (White

and Simms, 2003). The Roy White Extended algorithm uses a cross-correlation between the

reflectivity (reflection coefficients) computed and a seismic trace, autocorrelation of

reflectivity, and a noise factor. The extracted wavelet is multiplied by the reflection coefficients

(convolved) for the entire portion of the well that was logged and generates a synthetic

seismogram for the well. The synthetic seismogram was essential when performing the well-to-

seismic ties throughout the seismic volume. The synthetic seismogram was visually compared

to an appropriate seismic trace (proximal to the well) and bulk time shifts were applied to the

synthetic seismogram to best-fit the synthetic seismogram to the seismic data. A bulk shift is

applied when a reflector of similar amplitude in both the synthetic seismograms and the

seismic data is not aligned properly, the synthetic seismogram is shifted vertically to align with

the seismic data. Unaligned reflectors can be a result of the following factors: quality of the

logs, quality of the seismic data, processing of the seismic data, or other factors. This

completed the well-to-seismic data tie and allowed the formation tops to be interpreted in the

wells, which were then correlated to specific seismic reflectors throughout the seismic volume.

This study executed multiple well-to-seismic data ties throughout the seismic volume,

maximizing confidence during the interpretation of the seismic reflectors.

<u>Pseudo Wells</u>

As previously mentioned, the 28006 analog well was described in core and the formation and facies tops were identified. Utilizing the SON and RHOB logs, synthetic seismograms were created in Synthetic Seismic Profile Plot, a web application offered by the Kansas Geological Survey (KGS) (.kgs.ku.edu/software/SS/). This application allows the operator to generate synthetic seismograms, with a Ricker wavelet of different frequencies. This was critical to determine the frequency necessary for the synthetic seismogram events to correlate with the formation and facies tops. Synthetic seismograms were generated with 50 Hertz (Hz), 100 Hz, and 150 Hz wavelets and the results were compared with the refined formation and facies tops. A Ricker wavelet is a statistical wavelet that is typically used in this approach.

Three pseudo well locations were selected and evenly spaced between the 29073 and 29989 wells, shown in the map of view of the field in figure 12. Two SON and RHOB logs were created for each well (Well A, Well B, Well C). The pseudo logs start at the top of the Brown Niagaran and extended to the top of the Gray Niagaran. The RHOB values assigned to the logs were a result of averaging the RHOB logs from the 29073, 57916, and 29989 wells. Similarly, the SON values were an average of the SON logs from the 29073 and 29989 wells. These wells were selected because of their proximity to the cross-section and assumed to be representative. The SON and RHOB values extracted for averaging were specific to the formation or facies they corresponded to. A set of averaged SON and RHOB values for the Brown Niagaran, Reef Core, Coarse Skeletal, Bioherm, and Gray Niagaran were utilized for constructing the pseudo logs. The pseudo wells characterized based on the two geologic models previously created using a Rine (2015) approach and a Gill (1973) approach. Dependent on the location of the pseudo wells in

13

the models, the wells penetrate different predicted strata. For each pseudo well, a SON and

RHOB pseudo log was constructed using the appropriate averaged values for the strata they

penetrate, for each of the geologic models. The result is two sets of logs for each pseudo well

(i.e. Well A: Gill A logs and Rine A logs). Synthetic seismograms were then generated using the

KSGS software with a 100 Hz Ricker wavelet for each log set. The resulting synthetic

seismograms were then overlaid on the seismic data at their respective locations for

comparison.

Geophysical

3D Seismic Survey

Seismic reflections are the result of impedance contrasts at layer interfaces. The

resolution of the seismic data, is the ability to differentiate between unique geologic features.

In seismic reflection studies, resolution is referred to as: vertical (temporal) resolution and

lateral (spatial) resolution. Vertical resolution is the minimum difference in arrival times of two

reflections, at the surface, that allows the two reflectors to be detected separately (Sheriff,

1993). Lateral resolution is the minimum horizontal distance between two geologic objects,

which allows the objects to be imaged individually. The quality of the resolution is dependent

on the wavelength of the seismic signal. Wavelength is defined by: $\lambda = \frac{V}{F}$; where λ is the

compressional (p) wavelength; V is average velocity; F is dominant frequency (Figure 13).

Resolution deteriorates with depth due to longer wavelengths from increasing velocity and

lowering of frequency (Figure 13). Because the focus of this study is relatively deep in the

subsurface (~5000 feet or 1200 meters), visualization techniques and attribute tools were essential for displaying the seismic data.

Data can be visualized several ways to highlight geologic features. The seismic data for this study was loaded into the Schlumberger software Petrel project that also included the petrological data discussed above. Petrel, by default, uses a seismic data color template where red represents peaks and blue represents troughs. For this study the color table was reversed to reflect the US convention of normal polarity. Peak events, representing an increase in acoustic impedance, are shown as blue seismic reflectors. Consequently, red seismic reflectors represent a decrease in acoustic impedance, or troughs. To obtain geological control when interpreting reflectors, existing wells with good quality well-to-seismic ties were overlain on the seismic section. The formation tops derived from the borehole were displayed allowing seismic reflectors to be interpreted.

<u>Seismic Attribute Analysis</u>

To aid with interpretation, seismic attributes were utilized in addition to the well-to-seismic cross section ties. A Variance (edge method) attribute was utilized to identify the areal extent of the reef complex. The Variance attribute is a method patented by Schlumberger for imaging discontinuities in the horizontal continuity of amplitudes. Large signal variance often coincides with signal discontinuity that can have stratigraphic and structural origins, such as a reef complex (Toelle, 2012). Seismic variance was extracted from the "Monitor" survey.

An Instantaneous Frequency attribute was applied to the seismic volume and was a critical component when interpreting the reef architecture. The Instantaneous Frequency attribute calculates and displays the time derivative of phase. Mathematically it is:

$$w = d(phase)/dt \qquad (Equation\ 3)$$

This attribute is commonly used to estimate seismic attenuation. Seismic attenuation

has been shown in this reef to be associated with zones of high porosity, where high

frequencies are preferentially attenuated and low frequencies prevail (Toelle, 2012). Because of

the Brown Niagaran is a carbonate structure, the rock density varies minimally. However, the

internal facies of the Brown Niagaran express variations in porosity. A limitation considered

when utilizing this attribute is the resolution of the seismic data. This tool was found to be

useful for visualizing the angle of the reef's windward and leeward sloping surfaces.

To visualize the Brown Niagaran temporally, time-slices of the seismic data with a

Relative Acoustic Impedance attribute applied, were taken every 1 millisecond starting at the

base of the reef. Relative acoustic impedance is calculated by integrating the seismic trace and

passing the result through a low-pass filter. It is useful for indicating sequence boundaries,

unconformity surfaces, and discontinuities in the signal. The time-slices create a time-lapse

from the start of deposition (base) to the conclusion (top) of the Brown Niagaran formation.

This helped to understand how the Brown Niagaran developed laterally over time. Because the

Brown Niagaran has different acoustic properties than the adjacent formations (i.e. evaporites),

the carbonate buildup responds differently than the evaporites when displayed using a relative

acoustic impedance attribute. The presence of regional dip that was not accounted for when

extracting the time-slices. However, it was considered when interpreting the time-slices.

The Iso-Frequency Component attribute was utilized in conjunction with the Relative

Acoustic Impedance attribute. The Iso-Frequency Component attribute calculates the

contribution of an individual frequency to the make-up of the input seismic signal. This is useful

for isolating frequency dependent changes in the signal, such as stratigraphic thinning. It was also used for understanding the frequencies present at a given two-way travel time. In this study, 120 Hz frequency was measured at two time-slices, both through the Brown Niagaran. The extracted time-slice displaying the 120 Hz frequency contribution at 872 milliseconds was compared to the relative acoustic impedance time-slice at 872 milliseconds to observe correlations. Like the Relative Acoustic Impedance attribute, a limitation of the Iso-Frequency Component attribute is, the potential for artifacts when regional dip is a factor.

A Root-Mean-Square (RMS) Amplitude attribute was applied to the seismic survey. RMS Amplitude is the square root of the sum of the squared amplitudes, over the number of samples. Mathematically it is:

$$\sqrt{\frac{(\sum_i^n amp^2)}{k}} \quad \text{(Equation 4)}$$

The RMS amplitude aids in mapping geologic features that are isolated from background features by their amplitude response. This attribute can also be utilized to highlight facies changes and unconformities. This was important when analyzing the internal structure of the reef complex in the seismic profile.

Seismic Data Interpretation

Three basic methods were used to perform seismic horizon tracking in Petrel: Manual interpretation, Seeded 2D Autotracking, and Seeded 3D Autotracking. To maintain good quality control a combination of the methods was used. The seismic data quality determines which method will be applied. In areas of poor seismic data quality and reflector continuity manual interpretation was applied. Likewise, in areas of very good seismic data quality and reflector continuity, autotracking was utilized.

Petrophysical and Geophysical

In the Charlton 30-31 reef complex the density contrast between internal reef facies is minimal. As a result, at best subtle seismic signatures are expected within the reef interior. To identify the subtle seismic signatures within the reef, the seismic data was compared to the pseudo synthetic seismograms in this study. The overall geometry of the reef was investigated using the multiple seismic attribute responses and comparing them with the geologic models developed to determine which was most consistent. If the architecture and facies distribution in the seismic model appeared asymmetrical and had preferential distribution based on windward or leeward directions, Rine's model was considered appropriate. If the seismic data interpretations showed a symmetrical architecture with no predictable facies distributions, Gill's model was considered applicable.

CHAPTER III

RESULTS AND INTERPRETATIONS

Geophysical Logs

Displaying the GR log on an amplified scale (O to 50 API units) significantly improved the visibility of variation in the log signatures (Figure 14). Off-reef wells exhibited a practically identical signature and formation signatures were readily identifiable. Equivalently, the on-reef wells (analog well included) demonstrated similar GR signatures overall, comprised of unique individual formation signatures that were consistent for each well. Common signatures found in Rine (2015) were similar to the GR signatures in this study and the GR logs were interpreted

utilizing the unique formation and facies signatures from Rine (2015). Within the on-reef wells the Brown Niagaran formation displays minimal variation in the GR signature, which was expected of the carbonate buildup. To further investigate the facies interpretations within the Brown Niagaran formation, all the available wire-line logs for each on-reef well were displayed in separate tracks next to the GR log. Variation in rock characteristics not visible in the GR signature, were prominent in the SON, RHOB, and NPHI signatures. When the RHOB and NPHI logs were analyzed, discernible signatures were visible, but no applicable consistencies were observed across the wells. However, when the SON log was coupled with the GR, variation in the SON logs correlated well to the Bioherm and the Reef Core tops previously identified using the GR log. Across all SON logs, a noticeable increase in the SON signature and decrease in the GR signature, is present within the Reef Core. The Bioherm facies correlates to a slight increase in the GR signature and a decrease in the SON signature. The SON signature displays more variation than the GR signature within the Brown Niagaran and was used to reduce uncertainty in the initial facies interpretation.

The 5 wells located in off-reef locations were drilled as deep as the Gray Niagaran, as a result they penetrated the Brown Niagaran and the A-1 Evaporite. The lack of the Bioherm and the Reef Core facies in the Brown Niagaran and the presence of the A-1 Evaporite in off-reef wells, was expected. All 7 wells that were drilled on the reef (as well as the 28006 well), lacked A-1 Evaporite but the Bioherm and Reef Core facies were identified. Based on previous studies by Gill (1973) and Rine (2015), this was expected because the A-1 Evaporite pinches out near the base of the Brown Niagaran and the Brown Niagaran is comprised of Bioherm and Reef

Core facies. The available logs and their interpretations for the 5 wells used to construct a southwest to northeast transect, are shown in Figure 14.

Core Description

Following the formation and facies interpretations made with geophysical logs, interpretations were made based on observations in core. The cored interval for the 28006 well extended from a measured depth of 4671 to 4966 feet and nearly all the core was recovered for examination. The core was analyzed successively from the base to the top and all depths listed refer to the measured depth in feet.

<u>Bioherm</u>

The measured depth 4966'-4958', reacted weakly to acid, is very finely crystalline and gray to gray-tan in color, with a slightly mottled appearance. A change in color to brown is present from 4958'-4949' (Plate 1, Fig. A). This interval is fine to medium crystalline and is composed of pinpoint to micro-vug porosity (less than 0.25''). Continuing up section, 4949'-4925' is brown to grey and fine-medium crystalline. This interval is fractured, with salt infilling the fractures and partially infilling porous zones (Plate 1, Fig. B). Comprehensively, this section is fairly vuggy, has stromatactis texture, and contains a fair amount of fragmented skeletal remains including crinoids (Plate 1, Fig. C). The overall section (4966'- 4925') closely resembled the descriptions of Rine (2015) for the reef Bioherm facies. Rine (2015) described the Bioherm facies as having a mottled appearance and an abundance of crystalline dolomite with an abundance of stromatactis texture. Therefore, this interval was identified as the Bioherm facies.

Reef Core

The core remains dolomitized but the addition of brachiopod fragments at 4925', marks a potential facies change (Plate 2, Fig. A). A noticeable increase in vugs and porosity also initiates at 4925'. Good vuggy porosity resulting from generally smaller vugs and periodic brecciation continues up to 4880' (Plate 2, Fig. B). At 4880' a large coral is identifiable, and vugs become less frequent but larger in diameter (up to 0.75'') (Plate 2, Fig. C). Extending upward to 4719', the diameter of the vugs varies from pinpoint to large (0.25''- 1.25'') and the frequency of the vugs varies as well, resulting in good to very good porosity. High angle fractures were observed starting around 4831' and continuing up to 4744'. These fractures are commonly filled with calcite cements (Plate 2, Fig. D). Overall, from 4925' – 4719' the core has good porosity, high-angle fractured zones, brecciated intervals, skeletal fragments (identifiable: crinoids, brachiopods, and corals), and fluctuating vug size and prevalence. The presence of a mixed assemblage of organisms, vuggy porosity, and differing rock fabrics due to the complex environment during deposition, is consistent with the Rine (2015) description of the Reef Core facies. This led to the identification of the interval 4925'-4719' as the Reef Core.

Cyanobacterial Mats

A distinct change in the characteristic of the rock occurs at 4719'. Above this level the rock is comprised of dolomitized crinkly stromatolitic bindstone and stromatolitic conglomerate. The stromatolitic bindstone is dark brown in color, with little to no bioturbation or fragmented clasts (Plate 3, Fig. A). Typically, the stromatolitic bindstone is made up of thin laminae that appear to be in situ (Plate 3, Fig. B). Interbedded in this interval are stromatolitic conglomerates comprised of fragmented and brecciated stromatolitic bindstone (Plate 3, Fig.

C). Often the conglomerates occur at relatively high angles within the core (Plate 3, Fig. A). The occurrence of stromatolitic bindstone and stromatolitic conglomerates from 4719'-4714', overlying the Reef Core facies is consistent with what Rine (2015) describes as the Cyanobacterial Mats. Therefore, the last facies identified within the Brown Niagaran formation was interpreted as the Cyanobacterial Mats facies.

Thrombolitic Bindstone

An obvious change from stromatolitic bindstone (stratified internal fabric) to thrombolitic bindstone composed of irregular and patchy clotted internal fabric is observed at 4714' (Plate 3, Fig. D). The thrombolites have a mottled appearance and are darker brown with lighter tan cements. The thrombolitic bindstone is separated from the underlying stromatolitic bindstone by a sharp unconformable contact. The base of the A-1 Carbonate in Rine (2015) is comprised of irregular and patchy clotted internal fabrics, interpreted as the Thrombolitic Bindstone facies. This is consistent with what was observed in this study from 4714'-4690' and marks the beginning of deposition for the A-1 Carbonate formation. The Thrombolitic Bindstone facies is considered hereafter to be a part of the A-1 Carbonate.

Laminated Peloidal Wackestone

Another abrupt change in the core is observed at 4690'. Laminated peloidal wackestone that exhibits wavy and parallel laminations, extends from 4690' to 4685.5' (Plate 4, Fig. A). The wavy laminations are not crinkly like the laminations typical of stromatoporoids. The laminated peloidal wackestone is relatively flat lying at 4690' and transitions to much higher angle bedding near 4686.5' (Plate 4, Fig. B). Few scattered anhydrite nodules occur cross-cutting laminations and range in diameter (less than 0.25'' to 2.0''). This facies was identified in Rine

(2015) as the Laminated Peloidal Wackestone. For this study, the Laminated Peloidal Wackestone (4690'-4685.5') will be referred to as a member of the A-1 Carbonate formation.

Rabbit Ears Anhydrite

A marked change in lithology from dolomite to an anhydrite rich rock occurs at 4685.5' (Plate 4, Fig. B). The anhydrite interval extends from 4685.5' to 4671'. A gradational change is observed from massive anhydrite nodules at the base to smaller nodules near the top (Plate 4, Fig. C). The top of the section is dominated by dolomite and comprised of less anhydrite nodules that are slightly darker in color (Plate 4, Fig. D). This is interpreted as the Rabbit Ears Anhydrite facies due to its similarities with what is described in Rine (2015), a sharp contact between the Laminated Peloidal Wackestone and the presence of nodular anhydrite. This is the uppermost interval of the 28006 core and is included with the previous A-1 Carbonate facies, all three of which are referred to as the A-1 Carbonate formation going forward.

Facies Comparison

When compared, the facies interpreted from both the GR logs and the core were highly consistent. The GR log tops corresponded well with the core derived tops and increased the confidence of the facies interpretations for the Charlton 30-31 field. Figure 15 shows the 28006 well with the final facies interpretations, the GR log, and SON log to demonstrate the log signatures utilized to refine the facies interpretations for the Charlton 30-31 field. No inconsistences in the facies generated from geophysical logs, for the analog field, were significant enough to require revision of the initial GR signature interpretations for the Charlton 30-31 field. This finding was critical because, although the Charlton 30-31 field lacks core, the

interpreted formation and facies tops were confidently used in the geologic modeling of the

Charlton 30-31 field.

Geologic Model

Utilizing the formation and facies tops, two geologic models were developed.

Extrapolation between wells for the first model reflected the model proposed by Gill (1973)

(Figure 16-I). This model interpreted the Charlton 30-31 as having a relatively symmetrical

overall architecture with the internal distribution of the reef core being disrupted by

interfingering of coarse skeletal material. This model lacks windward and leeward facies. The

second model was built to reflect the Rine (2015) proposed model for pinnacle reefs. This

model of the Charlton 30-31 has asymmetrical overall geometry with predictable and

continuous internal facies. The Rine (2015) style model also includes windward and leeward

facies (Figure 16-II).

Well-to-Seismic Cross Section Ties

Wavelet analysis was conducted at locations within the seismic volume, proximal to the

wells that included SON logs. A deterministic method called the White's Extended algorithm

was used for the wavelet extraction (White and Simms, 2003), which includes the reflection

coefficients calculated from the SON and RHOB logs. A short time window was used for the

extraction of wavelets from the seismic data. Figure 17-I. shows the synthetic seismogram

generated with an extracted wavelet from the vicinity of the 33136 well. The short-windowed

wavelet was extracted from cross-line 53 over a 100 milliseconds window. This display also

shows the well-to-seismic tie developed with the resulting synthetic seismogram for the 33136 well. In the figure, blue corresponds to strong positive reflectors (peaks) and red represents strong negative (troughs) values. This tie was interpreted by me to be "good" in quality. That is, most seismic events align and the amplitudes are similar (Table 2).

Figure 17-II displays the same information as the previous figure but for the 29073 well and its well-to-seismic cross section tie on the cross-line 50. This well is located on the reef so, as expected, the reflectors do not resemble the synthetic seismogram generated for 33136 well. That is, the reflectors below the A-2 Carbonate are much subtler in this location. This tie was interpreted by me to be of "fair" quality because the events correspond well but the strength of the reflectors are not consistent with amplitudes in the seismic trace data (Table 2).

Figure 17-III shows the well-to-seismic cross section tie on cross-line 55 for the 29989 well. A wavelet was extracted over a short (100 milliseconds) window near the vicinity of the 29989 well and identical parameters for generating synthetic seismograms were used for the remaining wells with SON and pseudo RHOB logs within the seismic survey. The seismic events and reflector strengths correspond well in this tie and the quality of the tie is interpreted by me to be "good" (Table 2).

Seismic Data Interpretation

The well-to-seismic cross section ties identify the major reflection events associated with the formations of interest and provide the grounds for seismic horizon interpretation in this study. Horizon interpretations were made by manually stepping through each cross-line and in-line to maintain good quality control when tracing the reflectors. Interpretations within

the reef started at cross-lines and in-lines where well-to-seismic ties existed, which increased

the confidence of the interpretations. Horizon tracking started with the A-2 Carbonate

formation due to its strong reflectivity and continued down to the Gray Niagaran. Two

"random" lines through the seismic data shows these interpretations and display the well-to-

seismic cross section ties (Figure 18). A "random" line refers to a transect through the seismic

data, connecting selected wells, that does not follow a seismic data cross-line or in-line. The

off-reef formations demonstrate strong, flat-lying reflectors allowing for high confidence and

rapid interpretations. The A-1 Carbonate formation in the seismic signature near the reef has a

strong positive reflector at the base of the formation and a weak peak at the top. This is

expected when looking at the well logs and the variability in the SON and GR signatures (Figure

14). The A-1 Carbonate horizon was traced using the strong peak event at the base of the

formation. Because of the minimal contrast in density between the A-1 Carbonate and the

Brown Niagaran, the two formations are not discriminated on top of the reef in the seismic

data (Toelle, 2012). This could also be due to the A-1 Carbonate being below the detection limit

of the seismic data (too thin). For this study, the A-1 Carbonate horizon interpretations cease at

the base of the reef and do not continue on to the reef. From geophysical logs it is known that

this formation exists on top of the reef, but it is not visible in the seismic survey. The Brown

Niagaran is interpreted as the top of the reef, as shown in Figure 18. Two of the techniques

utilized when interpreting the Brown Niagaran were based on the number of peaks between

the A-2 Carbonate and the Gray Niagaran, as well as the truncation of the A-1 Evaporite.

Because of the lack of A-1 Evaporite in on-reef wells, the A-1 Evaporite is interpreted as

truncating near the base of the Brown Niagaran. When the strong reflector associated with the

A-1 Evaporite disappears, that indicates the point where the reef edge begins. Utilizing multiple well-to-seismic cross section ties in combination with a good quality seismic survey, allowed for confident interpretations of horizons.

Seismic Attribute Analysis

Seismic attributes extracted from the seismic data where crucial during the interpretation of the seismic data. Multiple attributes were utilized to display the frequency and amplitude variation throughout the seismic survey that revealed features that would not have otherwise been observed. A time-slice was extracted at the top of the A-2 Carbonate using a Variance attribute (Figure 19). This time-slice clearly displays the boundary of the reef, shown in the figure as the bright blue signal. This tool not only showed where the reef buildup begins, it also led to a more detailed interpretation of the reef. That is, the time-slice shows that the northern portion of the reef is characterized by a more continuous signal than the southern portion. This suggests that the Charlton 30-31 field is composed of two reefs, not just one individual reef (Figure 19-II).

The Instantaneous Frequency attribute was applied to the seismic data. The seismic data was visualized in two cross-sections, one from southwest to northeast and the other from west to east. Similar responses for the windward slopes in the cross-sections were observed, the same is true for the leeward slopes (Figure 20). The windward slopes (east & northeast) display a sharp almost vertical change in signature going from blue-green-yellow blotches (on-reef) to a more continuous blue signature (off-reef) in the cross-sections. The cross-sections show a more gradual sloping change in the signal on the leeward side of the reef (west &

southwest). The specific angle of the slopes is not known but a qualitative analysis comparing the windward and leeward slopes, reveals clear differences. This led to the interpretation that the Charlton 30-31 reef was affected by the paleo-wind during deposition, developing a steeper windward slope and a more gradual leeward slope. The signal from within the reef displays no consistency laterally or vertically. The Instantaneous Frequency attribute also reveals the frequencies present within the reef, showing frequencies from approximately 100 Hz and less (Figure 20).

Another seismic attribute extracted was the RMS Amplitude. When displayed in the southwest to northeast cross-section a similar response to the instantaneous frequency signal is observed (Figure 21). In transition from on-reef to off-reef, the slope angle for the windward side of the reef is abrupt and obvious. The signal change is much more disrupted on the leeward side of the reef and shows a more gradational change in signal. The signal from within the reef is highly variable and shows no consistent signal changes laterally or vertically.

A time-slice was extracted from within the Brown Niagaran utilizing the Iso-Frequency Contribution attribute. Figure 22-II shows a semi-circular portion at the northern most extent of the reef having only a fraction of 120 Hz frequency contribution compared to the reef immediately surrounding the semi-circle. The large-scale signal change from northeast to southwest (resembling stripes in Fig. 22-II) is the result of regional dip. This attribute is considered useful on a localized scale because the regional dip is very low angle and its effects are only expected on the large-scale. A second, shallower time-slice was extracted from near the top of the Brown Niagaran to determine if this local structure was present in the signal and

the figure shows it is not (Figure 22-I). This further supports the interpretation that the semi-circle observed at the top of the Brown Niagaran is not an artifact of the seismic data.

A time-lapse of the Brown Niagaran was created using 7 time-slices extracted with the Relative Acoustic Impedance attribute. Starting at the base of the Brown Niagaran a time-slice was extracted every 1 millisecond going up through the Brown Niagaran and ending at the top of the formation (Figure 23). This revealed a semi-circular anomaly in the signal at the base of the formation (878 millisecond). This semi-circular anomaly is increasingly merged with the proximal anomaly to the southwest as the time-lapse continues upward to the top of the Brown Niagaran formation. The semi-circular anomaly resembles the semi-circular anomaly observed in the Iso-Frequency Contribution attribute. This resemblance decreases the uncertainty of this anomaly being an artifact of the regional dip influence on the time-slice. Thus, I interpret the semi-circular anomaly as a smaller individual carbonate build up, that over time merged with a larger carbonate buildup to the southwest. In other words, the Charlton 30-31 reef had multiple growth stages and the Reef Core facies is expected to be discontinuous, resembling the internal facies distribution proposed by Gill (1973). A regional scale background variation in the signal is present in the time-slices and is the result of regional dip of the basement from northeast to southwest at the time of deposition.

Pseudo Wells

The pseudo well (Well A, Well B, & Well C) locations and the predicted strata they penetrate are shown in Figure 24. Synthetic seismograms were generated from pseudo logs developed to reflect these stratigraphic changes. A 100 Hz Ricker wavelet was utilized because

it was the lowest frequency wavelet that produced a synthetic seismogram with a signature

that correlated well, with the formation and facies tops (see Figure 15). After producing the

pseudo synthetic seismograms, the three pseudo wells and their respective synthetic

seismograms were overlaid on the seismic data in the southwest to northeast cross-section

(Figure 25). Little to no variation is present between the Gill (1973) and Rine (2015) synthetic

seismograms for each well. The largest degree of variation is in pseudo Well B, where the Gill B

synthetic seismogram displays two subtle events within the Brown Niagaran (Figure 26). When

Well B is overlaid on the seismic data, the peaks in the synthetic seismogram are interpreted by

me to have a "fair" correlation with the seismic events in the vicinity (Table 2). The synthetic

seismograms for wells Well A and Well B show little to no resemblance with the seismic

signature and correlations are interpreted by me as "poor" (Table 2). The absence of

consistency between the pseudo synthetic seismograms and the seismic data is likely a result of

the internal facies distributions projected in the model lacking the same variability displayed in

the seismic survey. Despite the lack of consistency, both the Gill (1973) based model for the

Charlton 30-31 and the seismic survey, display variability within the reef interior.

CHAPTER IV

CONCLUSIONS

To conclude this study, it is appropriate to revisit the fundamental research questions

that were entertained throughout the study. The first question asks: *Is the seismic data*

resolution fine enough to detect internal reef architectures within the seismic survey utilized in

this study? This question was investigated subsequent to identifying the reef complex and the associated formations in the seismic survey. The instantaneous frequency and iso-frequency component attributes reveal the range of frequencies present within the reef. The frequency of the seismic data dictates the resolution. In this study, the reef internal frequencies were estimated to be 100 Hz and less, based on the seismic frequency attributes.

After producing synthetic seismograms for the cored 28006 well, it was determined that 100 Hz or greater resolution was necessary to identify the internal reef facies. The pseudo synthetic seismograms produced for the three pseudo wells were developed using a 100 Hz Ricker wavelet. The majority of the synthetic seismograms (4 of 6) displayed little to no variability within the Brown Niagaran. Synthetic seismograms showing variability correlated poorly with the seismic events when overlaid on to the seismic data cross-section. It is assumed that the resolution of the seismic data is below the detection limit for the internal facies and frequencies of greater than 100 Hz are necessary to discriminate facies within the reef interior.

The second fundamental research question was: *Do either of the published static geologic models reflect the reef geometry observed in the 3D seismic survey?* The initial stage in evaluating this question was using the refined formation and facies tops to develop two geologic models, one to reflect the Gill (1973) model and the other to reflect the Rine (2015) model. These models were the groundwork for developing three pseudo wells that penetrate the Charlton 30-31 reef. Pseudo logs were developed to reflect the predicted strata they penetrate, based on each model. The geologic models and their differing facies distributions could then be expressed using the pseudo synthetic seismograms. The internal distributions of the geologic models were represented by synthetic seismogram events and compared to the

events in the seismic survey. The comparison revealed no significant correlations and led to a second approach used to address the internal facies geometries.

The next approach was to examine the Brown Niagaran temporally, utilizing time-slices extracted from the seismic data with a relative acoustic impedance attribute applied. The time-slices created a time-lapse from the initiation to the ceasing of the Brown Niagaran formation. This method revealed more than one initial build-up, which merged over the duration of the time-lapse into one large build-up. This suggests that the reef had multiple growth stages and presumably unpredictable and discontinuous internal reef facies. Because of the lack of predictability of facies patterns within the reef, it is assumed that the Gill (1973) model is a better representation of the facies distributions, within the Charlton 30-31 reef.

When investigating the overall architecture of the Charlton 30-31, seismic attributes were pivotal. The iso-frequency attribute when visualized in two different cross-sections through the reef revealed a much steeper slope on the windward side of the reef and a more gradual slope on the leeward side. When observed in cross-section with an RMS amplitude attribute applied, the same was true, the windward side was much steeper than the leeward side. This asymmetrical overall architecture of the Charlton 30-31 reef, reflects the Rine (2015) model.

The final fundamental research question was: *What are the characteristics of the off-reef seismic signatures in this seismic survey?* This question was examined peripherally while investigating the prior two questions. When interpreting the seismic horizons, off-reef strata were relatively flat lying and had strong reflectors, allowing for rapid interpretations. This also allowed the reef boundary to be easily recognized when a variance attribute was applied, and a

time-slice through the build-up was extracted. Near the reef, the A-1 Carbonate formation's

signature is less distinct and transitions into multiple weak reflectors. The disrupted seismic

signal is interpreted to be the result of what Rine (2015) calls the Windward Reef Talus or

Windward Flank. The strong A-1 Evaporite formation reflector truncates into the reef build-up

as expected and was beneficial for identifying the reef boundary marked by the terminated

reflector.

The key observations in this study are: attribute analysis was instrumental in studying

the Charlton 30-31 field, it is possible to define the overall architecture and shape of the reef

complex, and the internal facies geometries cannot be defined with certainty, due to the

resolution of the seismic data. However, multiple attribute methods suggests an unpredictable

and variable internal character. The internal facies distribution show variability and no

predictability, this is consistent with the Gill (1973) model. The Charlton 30-31 reef has an

overall asymmetrical geometry, with a steeper windward slope and a more gradual leeward

slope, this is consistent with the Rine (2015) model. This study demonstrates the value of 3D

seismic reflection data when investigating the pinnacle reefs in the Michigan Basin.

TABLES

Table 1. Available Well Data

Information	28576	29989	40008	30203	57916	32605	29073	59048	32506	33136	30901	28006
					Charlton 30-31 Field							Charlton 4 Field
Gamma ray	X	X	X	X	X	X	X	X	X	X	X	X
Density			X	X	X	X	X					X
Sonic		X					X			X	X	X
Neutron φ		X										X
Core	X											X

Table 2. Well-to-Seismic Tie Quality and Criteria

Well-to Seismic Tie	
Quality	**Criteria**
Good	Events align/amplitudes are similar
Fair	Events align/amplitudes aren't similar
Poor	Events don't align/amplitudes aren't similar

FIGURES
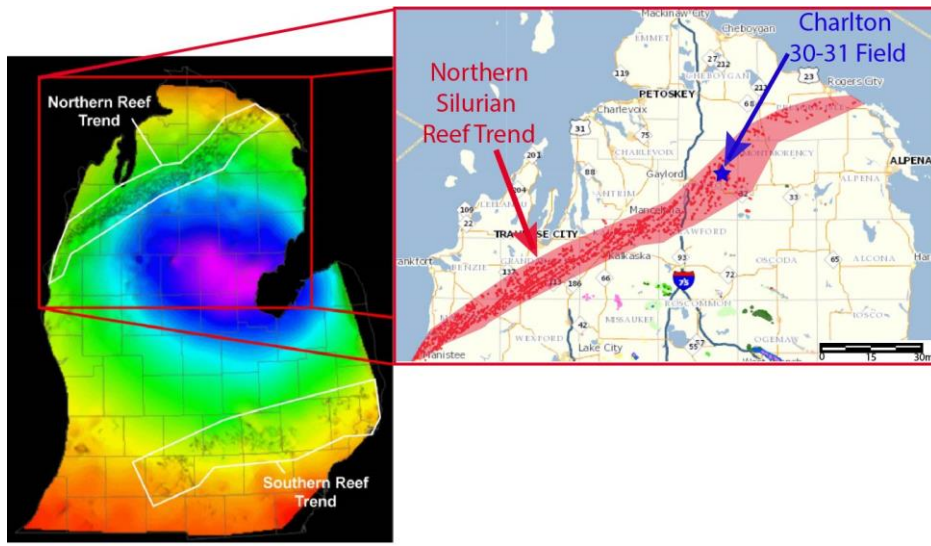
Figure 1. The left image shows the depth to the Brown Niagaran in the Michigan Lower peninsula; hot colors are shallower and cold colors are deeper. The right image shows the location of the Charlton 30-31 field in Otsego, County. (modified from Toelle et al, 2008; www.deq.state.mi.us/GeoWebFace/)

Figure 2. The chronological stacking order of the Silurian formations. (Fig 1.2 from Rine, 2015)

I. DIRECT

(A) Boundary Configuration

(B) Internal Patterns

II. INDIRECT

(A) Effects

(B) Basin Architecture
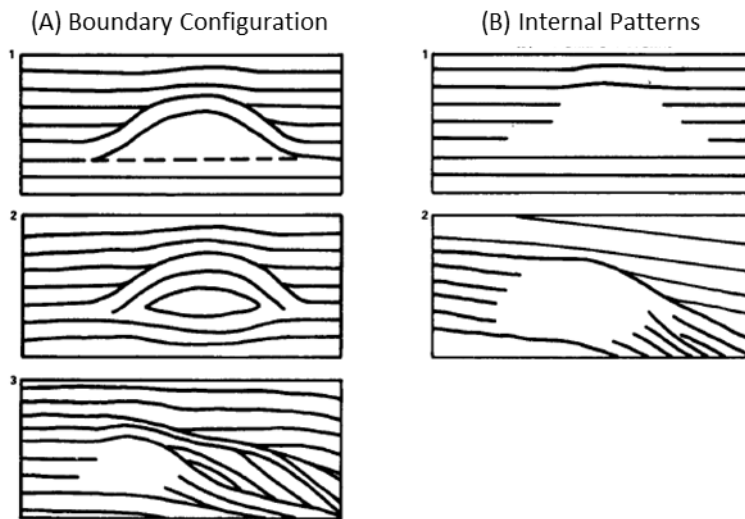
Figure 3. Bubb & Hatlelid (1978) criteria for recognizing carbonate buildups. (I-A) includes the criteria for directly outlining buildups due to overlying reflections on to buildup and onlap reflections, (I-B) shows patterns of facies changes internally, (II-A) shows indirect criteria: drape, velocity anomalies (pull-ups), and spurious events, (II-B) shows basin positions that are favorable for buildups. (Fig. 3 from Bubb & Hatlelid, 1978)
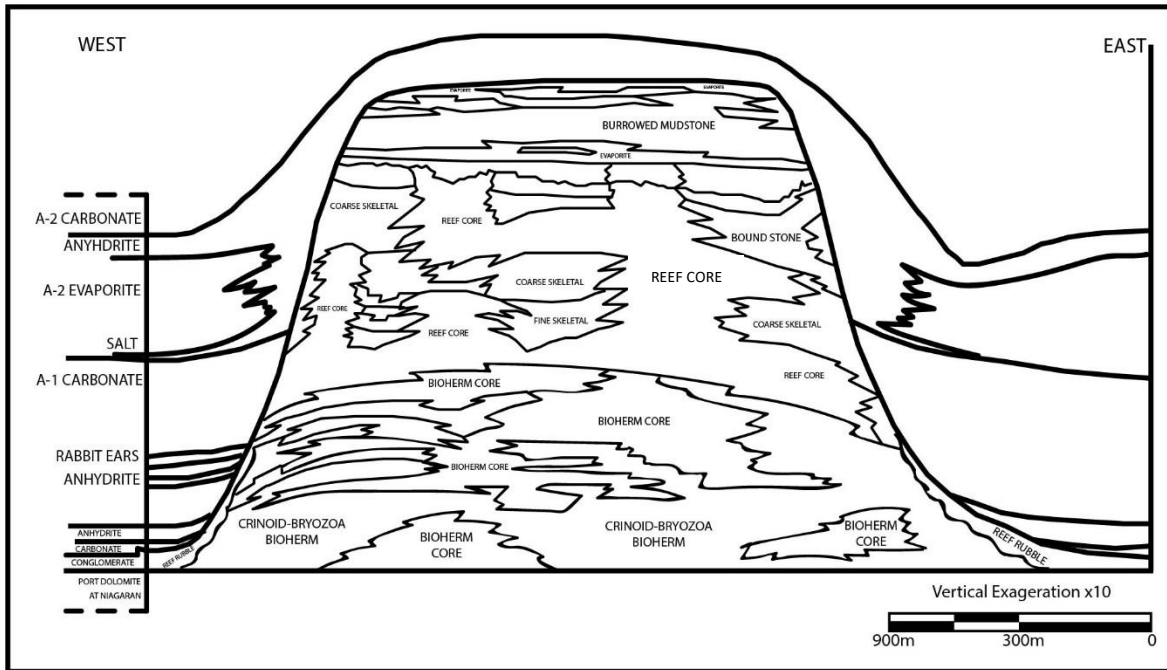
Figure 4. Gill's geologic model shows symmetrical architecture with unpredictably distributed, internal facies. (modified from Gill, 1973)
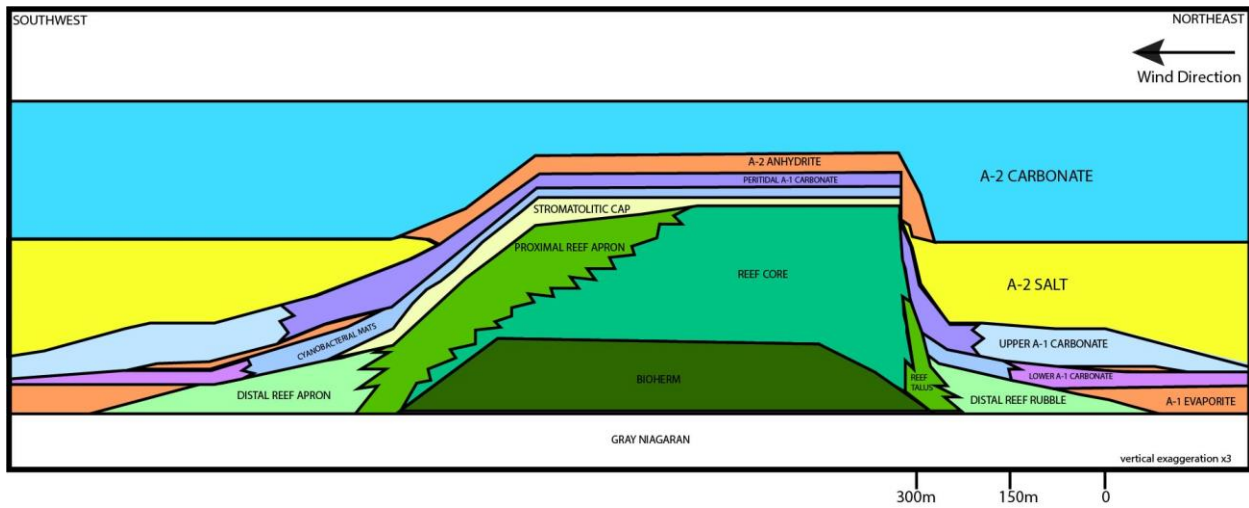
Figure 5. Rine's geologic model shows asymmetric architecture with predictable facies distributions; paleowind is the primary control on facies distributions. (modified from Rine, 2015)

Figure 6. An aerial view of the Charlton 30-31 field, the grey polygon outlines the reef and the wells are labeled with their respective permit numbers.

Figure 7. The location of the analog field (Charlton 4 field), with respect to the Charlton 30-31 field. (www.deq.state.mi.us/GeoWebFace/)
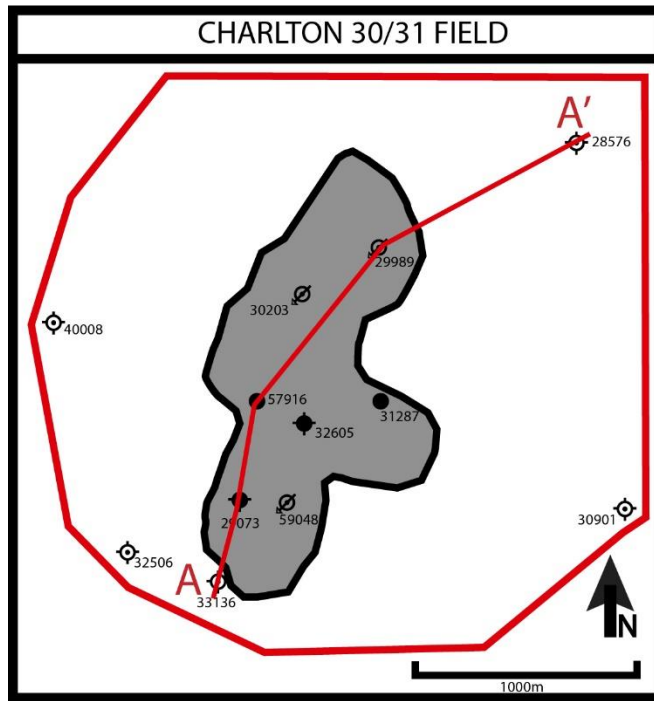
Figure 8. The red line (A-A') represents the cross-section used for developing the geologic models.
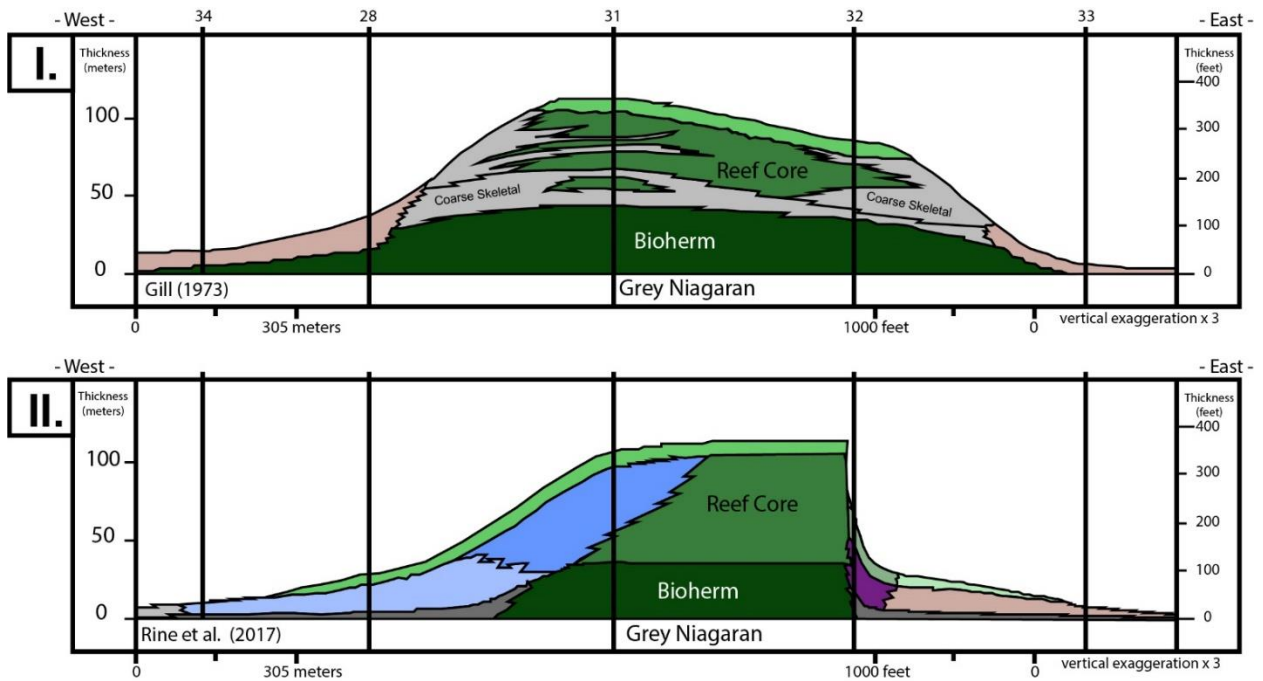
Figure 9. The top model resembles the interpretations made by Gill (1973) of the Belle River Mills reef and the bottom model is Rine et al. (2017) interpretations of the same reef. (modified from Rine et al. 2017)
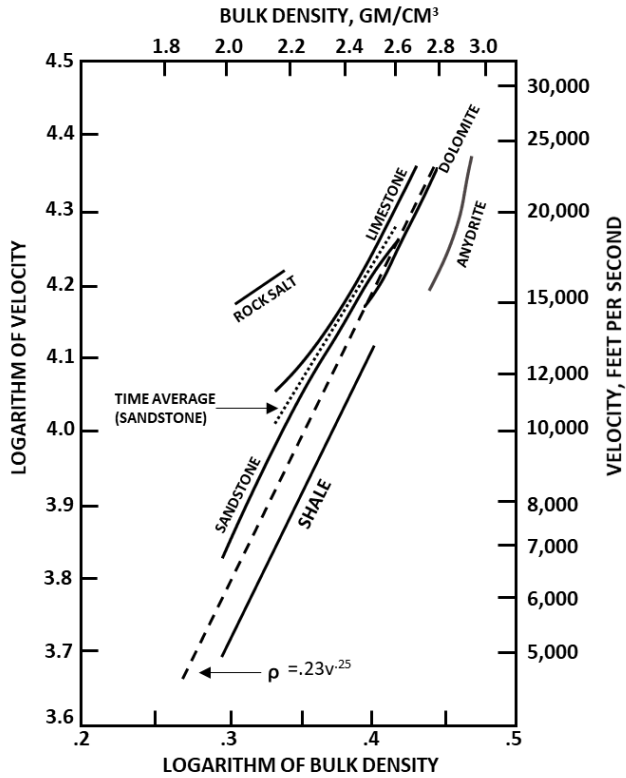
Figure 10. Velocity – density relationship in rocks of different lithology (Figure 1. from Gardner et al., 1974)
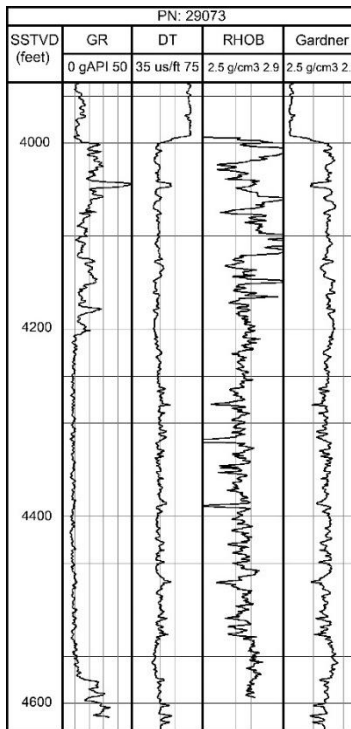
Figure 11. The results of producing a RHOB log using the Gardner equation and comparing it with a measured RHOB log. (SSTVD: Subsea True Vertical Depth, GR: Gamma-Ray, DT: Sonic Travel Time, RHOB: Bulk Density)
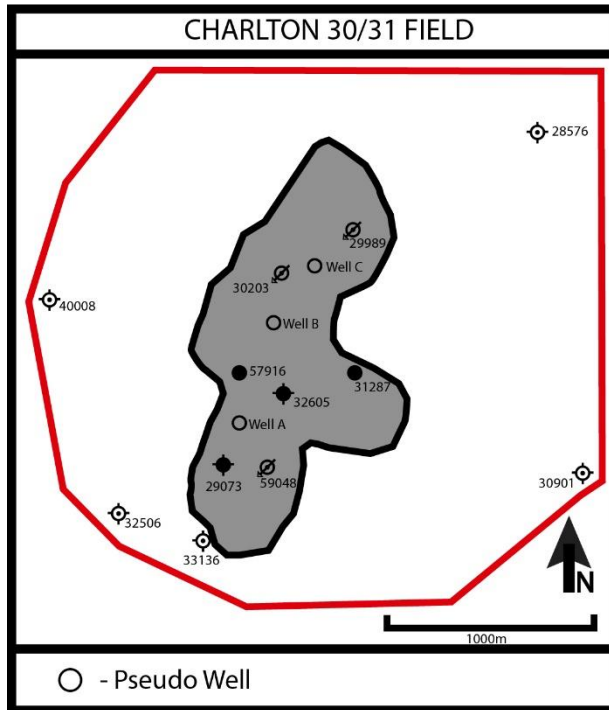
Figure 12. The location of 3 pseudo wells represented by open circles.
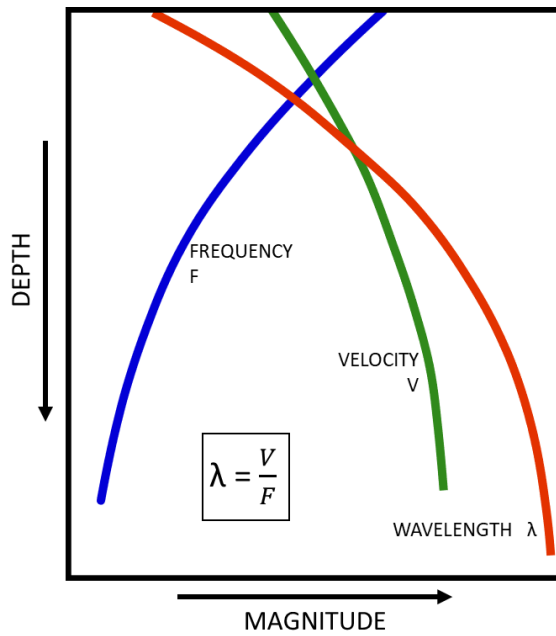
Figure 13. The character of sonic waves in the subsurface with increasing depth, wavelength controls the resolution of the seismic data. (modified from Brown, 1996)
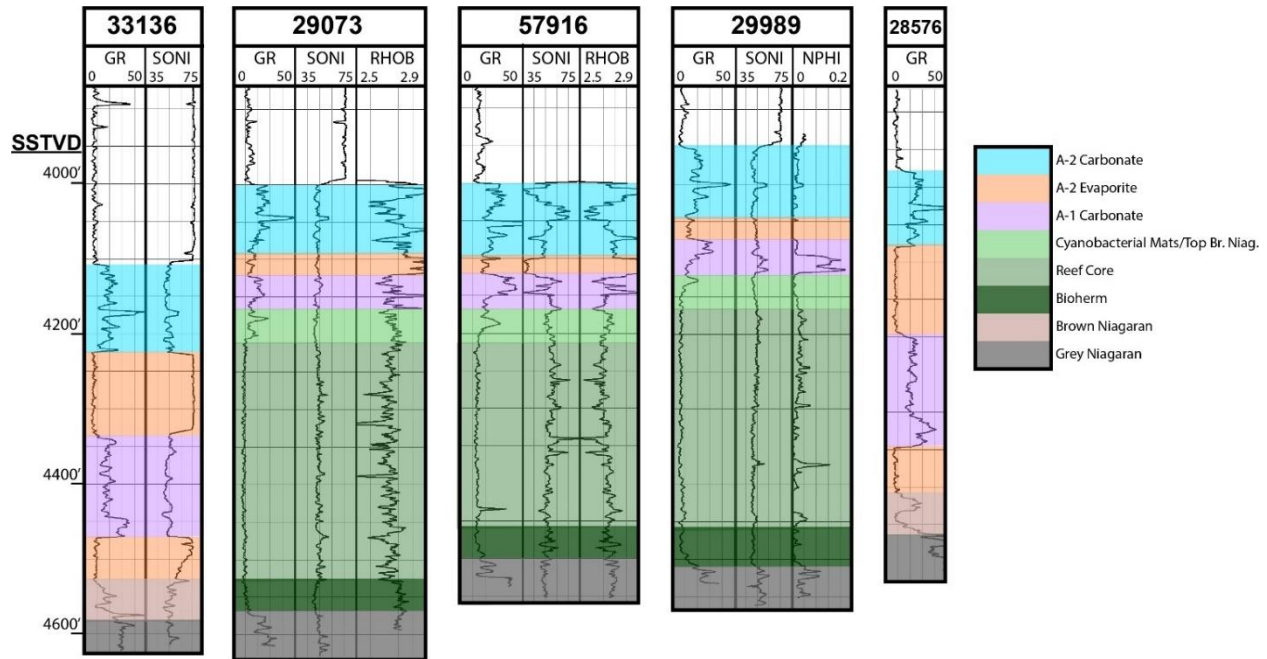
Figure 14. The 5 wells used in the SW-NE cross-section and their respective logs. (SONI: Sonic, NPHI: Neutron Porosity, Remaining abbreviations refer to previous figures)
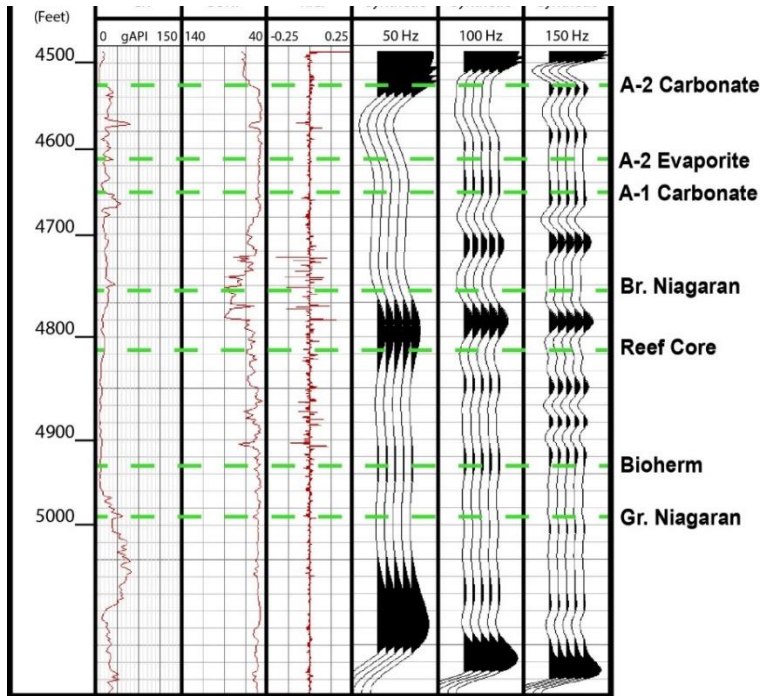
Figure 15. The final formation and facies interpretations made after comparing the facies from log and facies interpreted from core; also shown are the 3 synthetic seismograms produced for this well. (MD: Measured Depth, R.C.: Reflection Coefficients, Remaining abbreviations refer to previous figures)
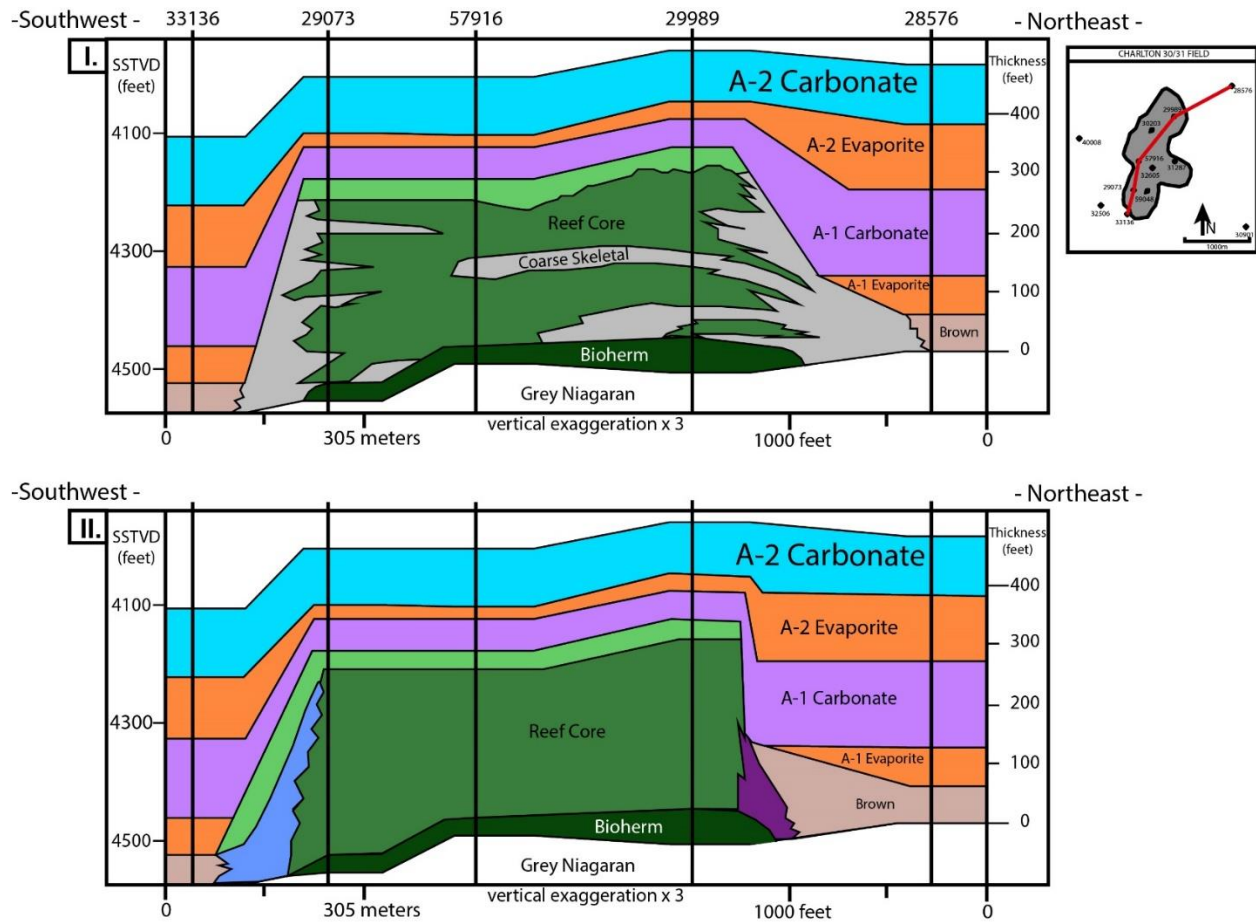
Figure 16. Two geologic models developed based on Gill (1973) (top) and Rine (2015) (bottom), these models use the 5 wells from the SW-NE cross-section.
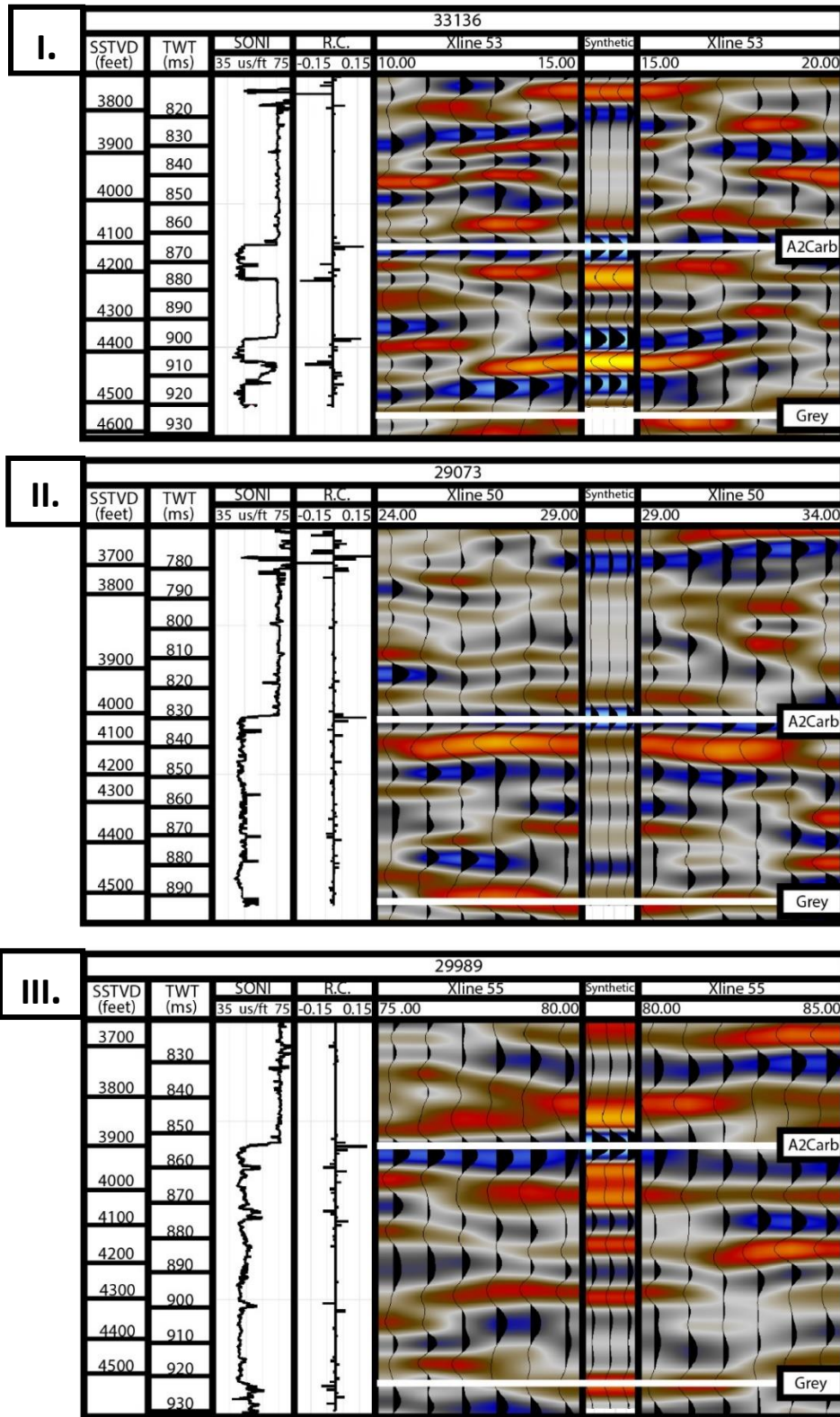
Figure 17. Well-to-seismic ties for the off-reef well 33136 and the on-reef wells 29073 and 29989. (TWT: Two-way Time, Xline: crossline, Remaining abbreviations refer to previous figures)

47
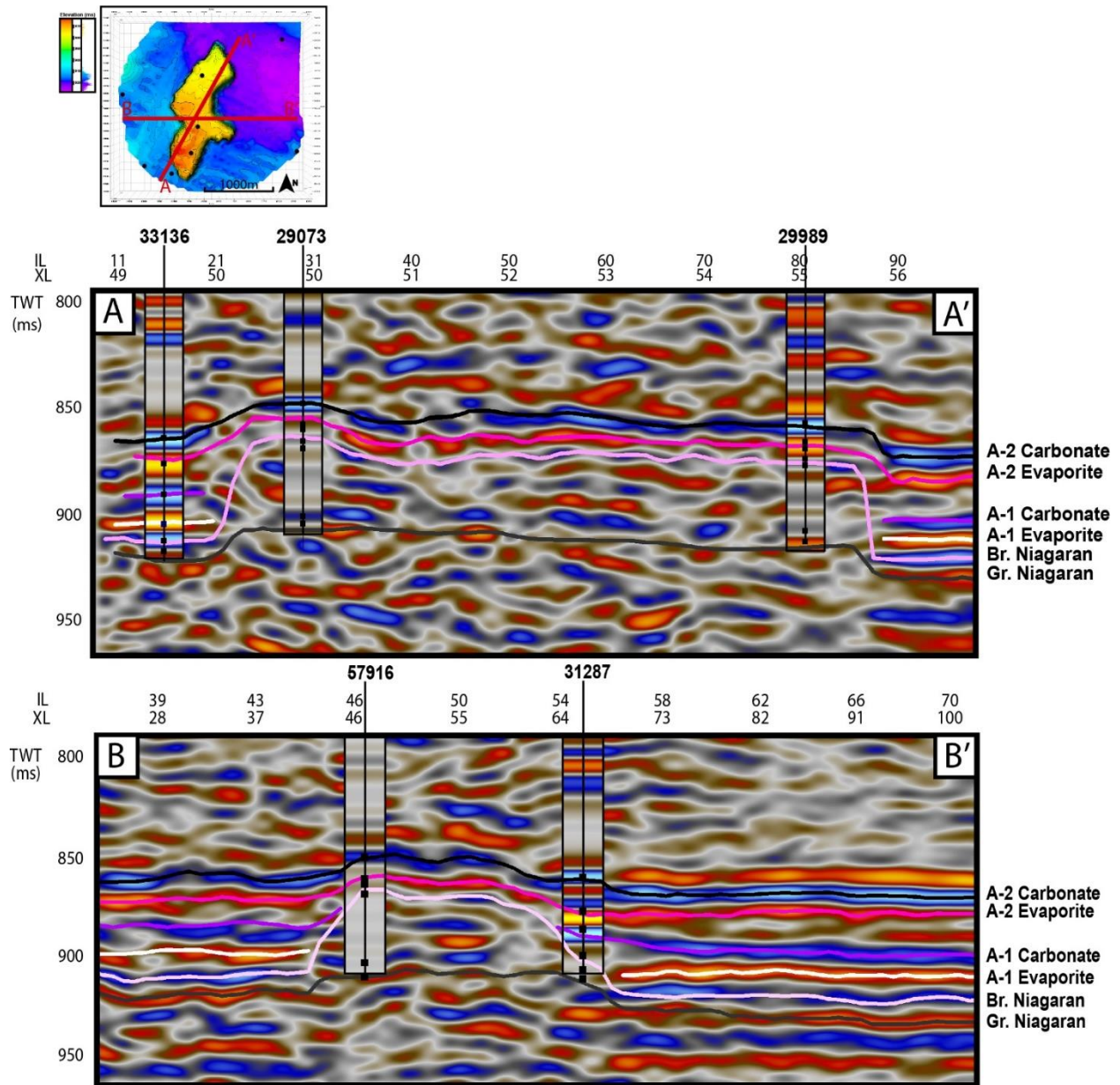
Figure 18. Cross-sections through the seismic data with the synthetic seismograms overlaid on them; also shown are the seismic horizon interpretations made for this study. (IL: In-Line, Remaining abbreviations refer to previous figures)
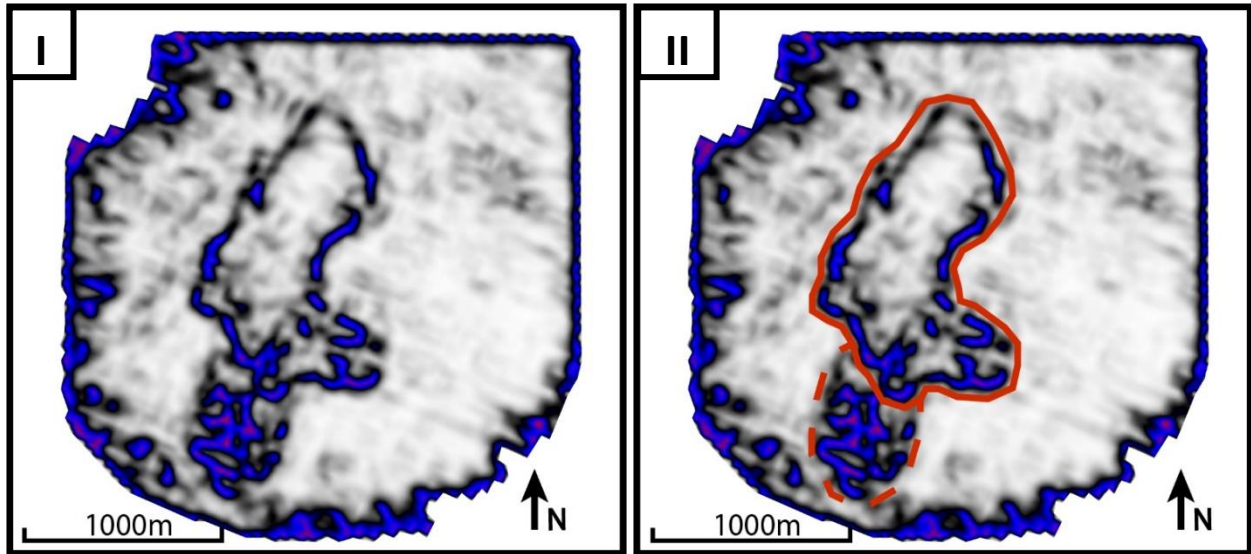
Figure 19. Time-slice extracted from the top of the A2 Carbonate using a variance attribute; Fig. 19-II is one interpretation of the Charlton 30-31 reef, suggesting there are two individual reefs.
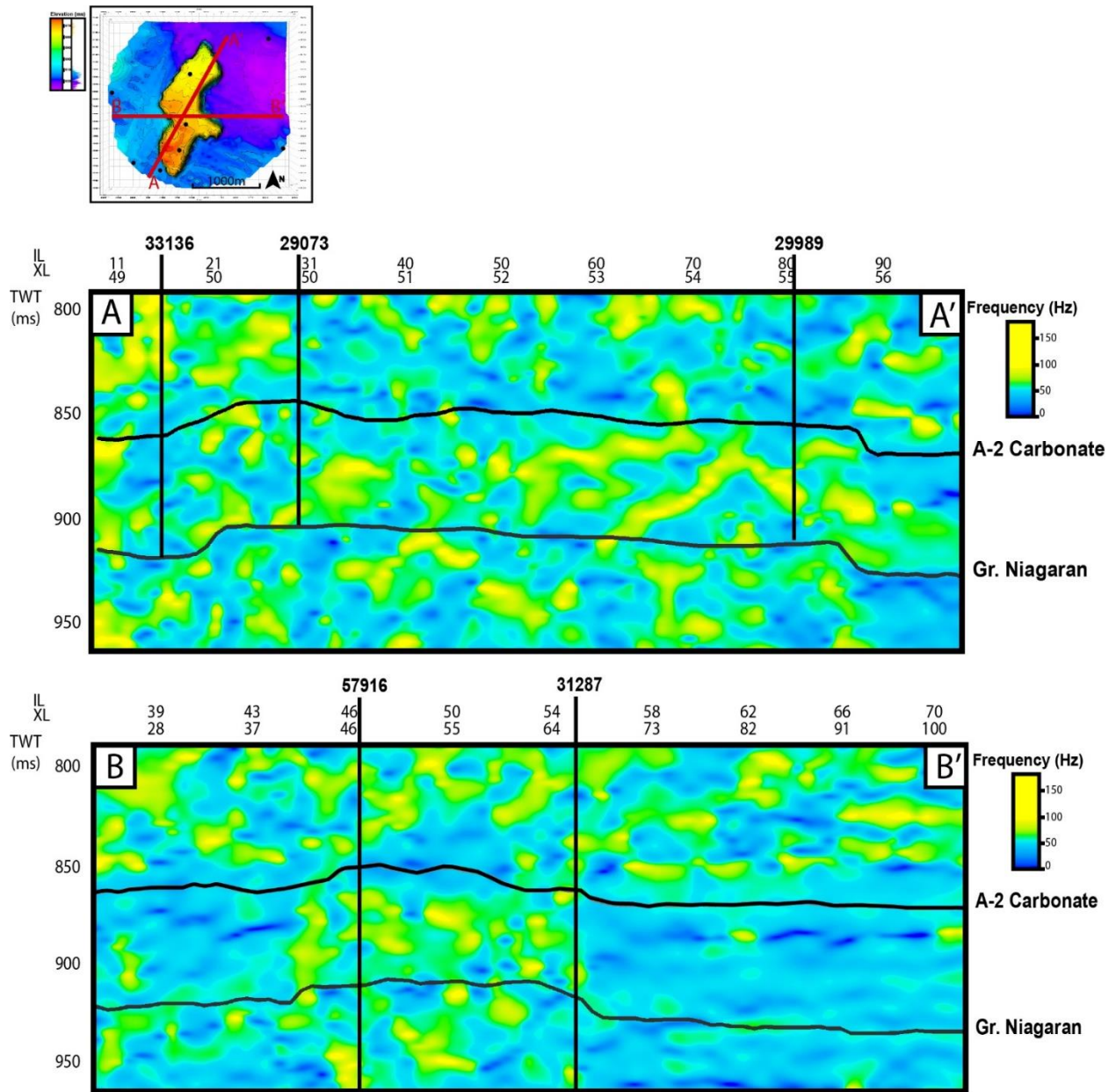
Figure 20. Two cross-sections with the Instantaneous Frequency attribute applied, utilized to observe the relative angle of the slopes of the Charlton 30-31 reef. (Refer to previous figures for abbreviations)
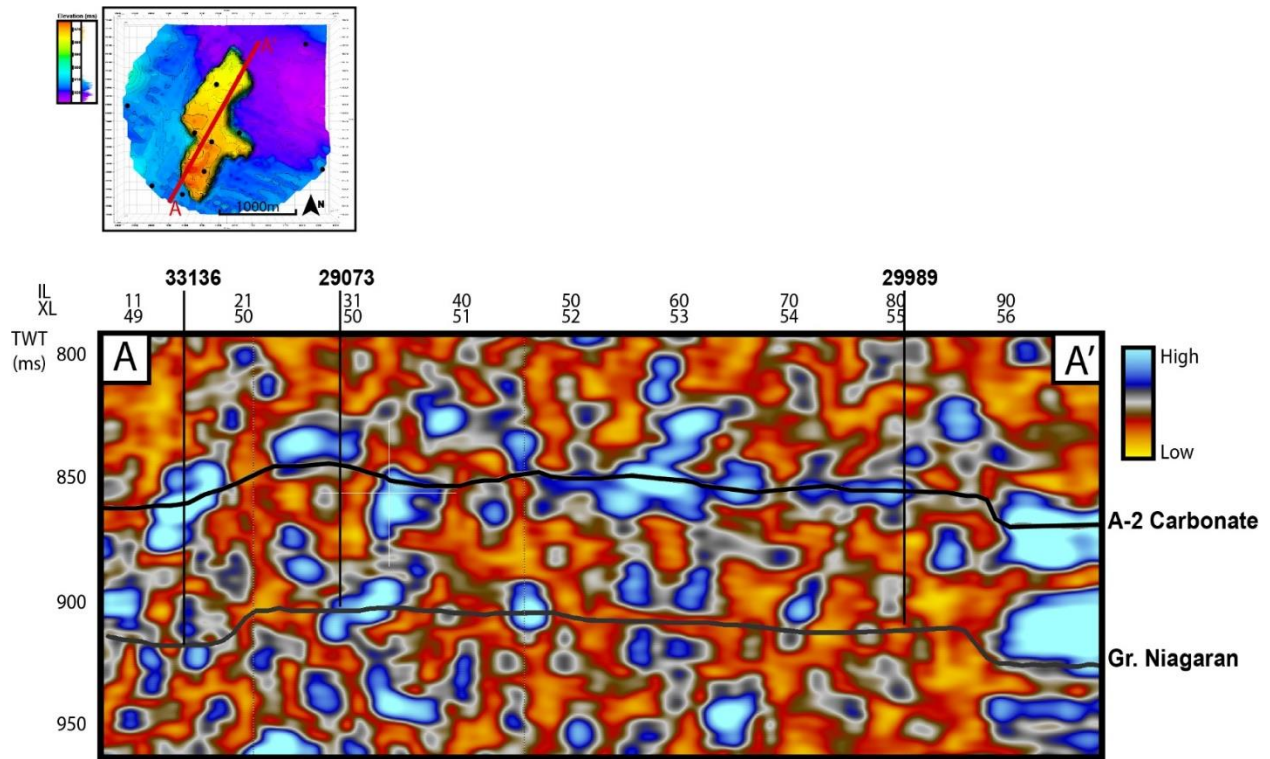
Figure 21. Cross-section through the seismic data with the RMS Amplitude attribute applied, utilized to observe the signal change from within the reef to off-reef data. (Refer to previous figures for abbreviations)
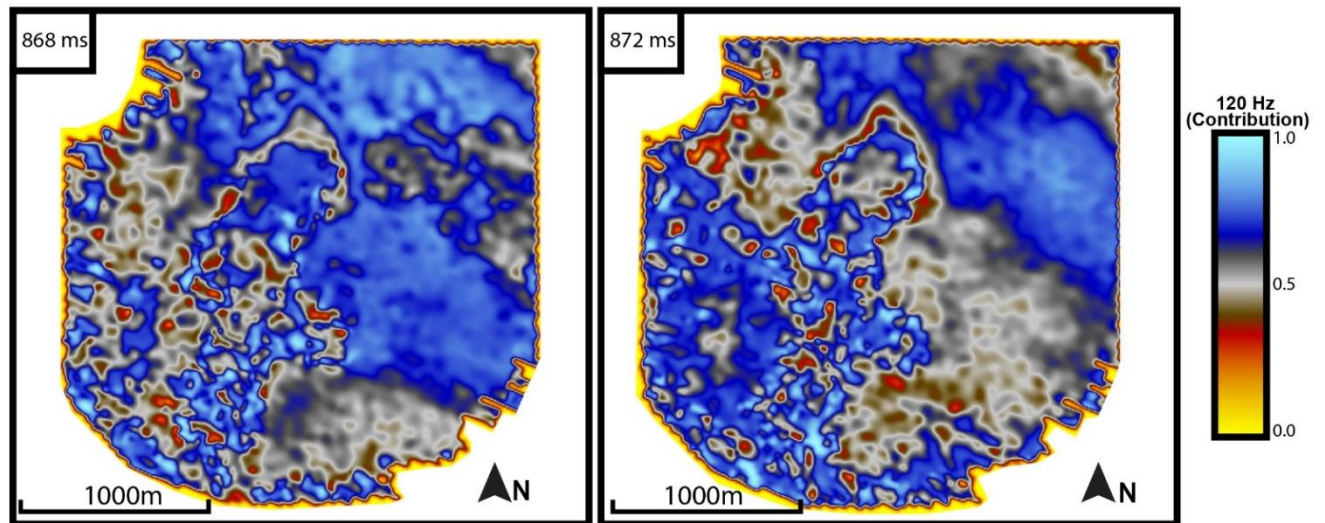
Figure 22. Two time-slices extracted from within the Br. Niagaran, with the Iso-frequency Contribution attribute applied to the seismic data.
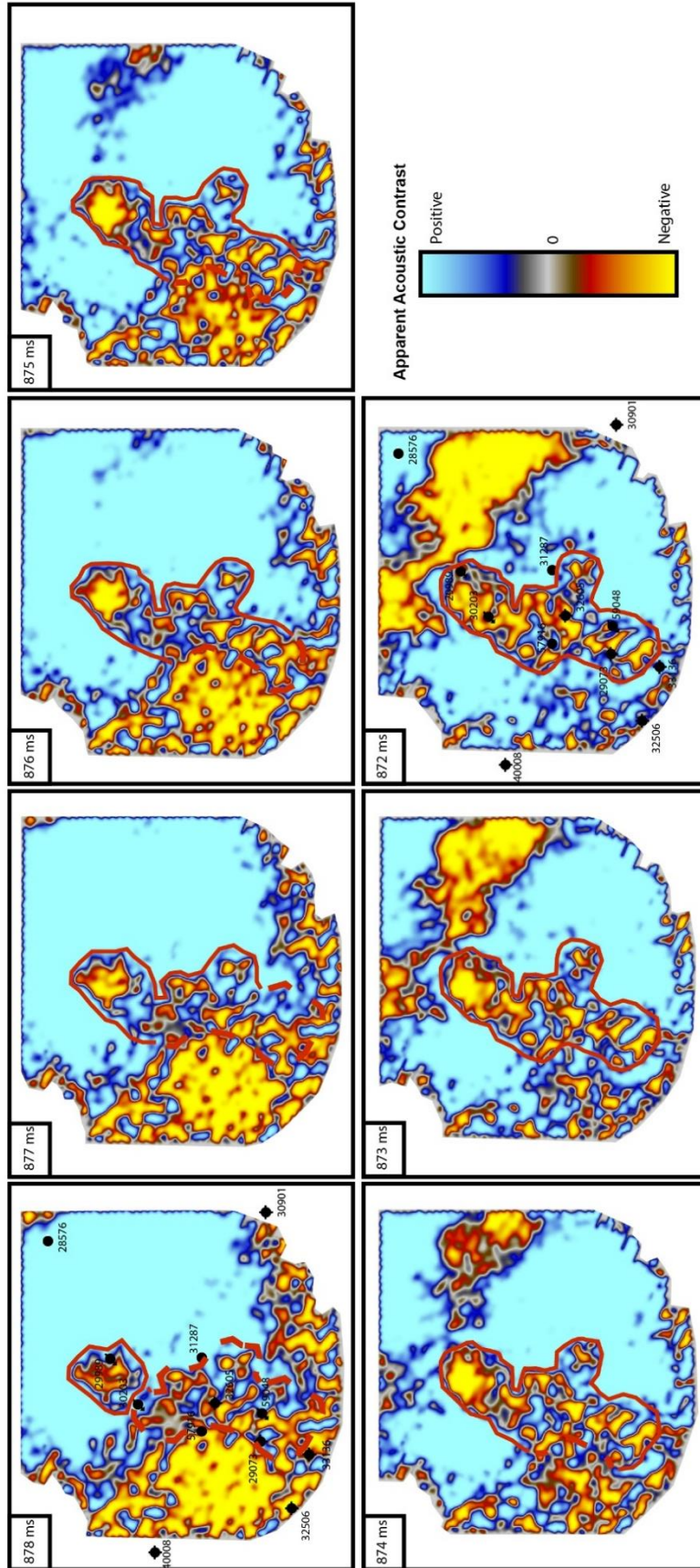
Figure 23. 7 time-slices extracted from within the Br. Niagaran, with the Relative Acoustic Impedance attribute applied to the seismic data; the red lines outline the interpretations made for each time-slice.

52
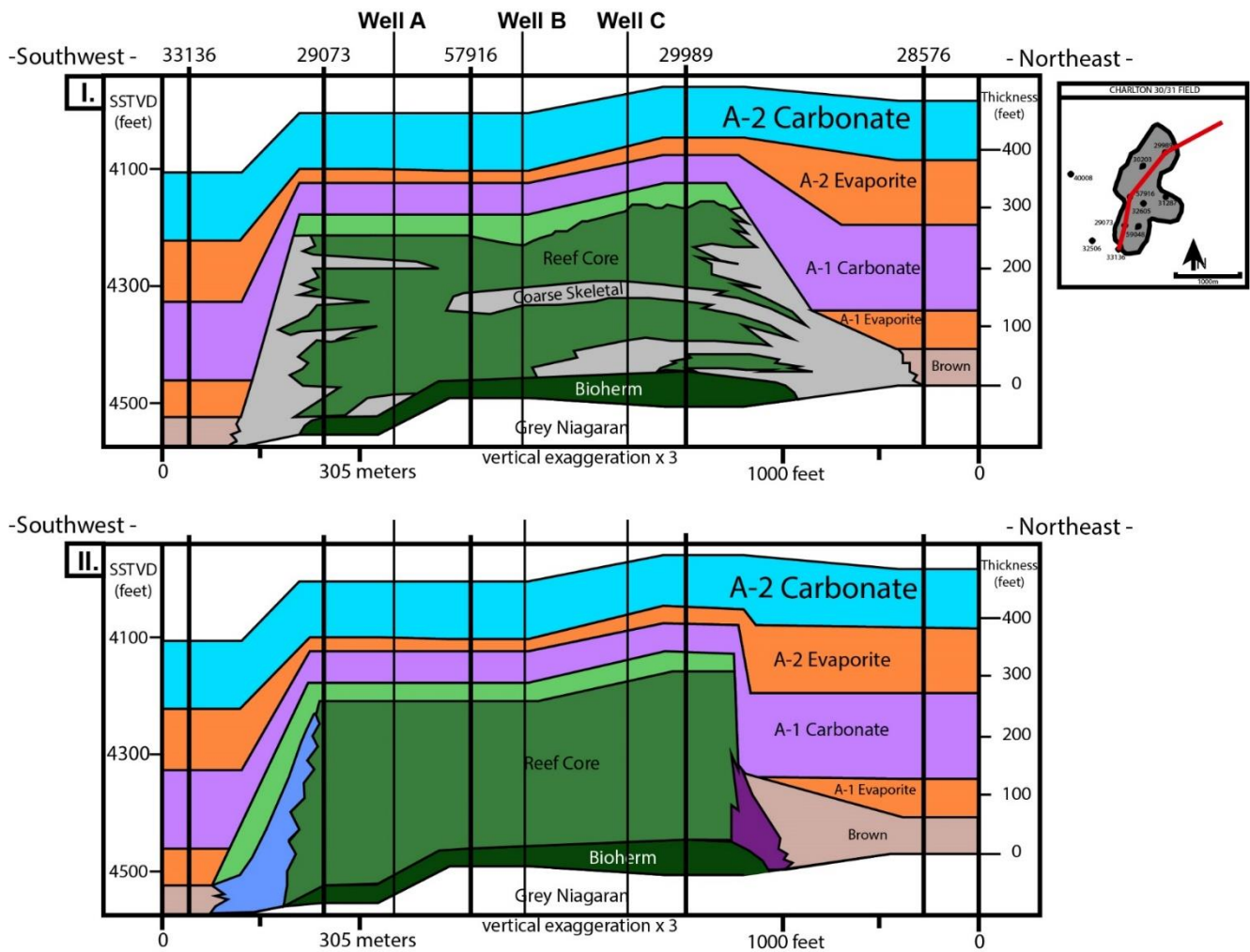
Figure 24. The pseudo wells (Well A, Well B, and Well C) overlaid on the geologic models developed earlier in this study; the predicted strata the pseudo wells penetrate are the basis on which the pseudo synthetic seismograms are developed. (Refer to previous figures for abbreviations)
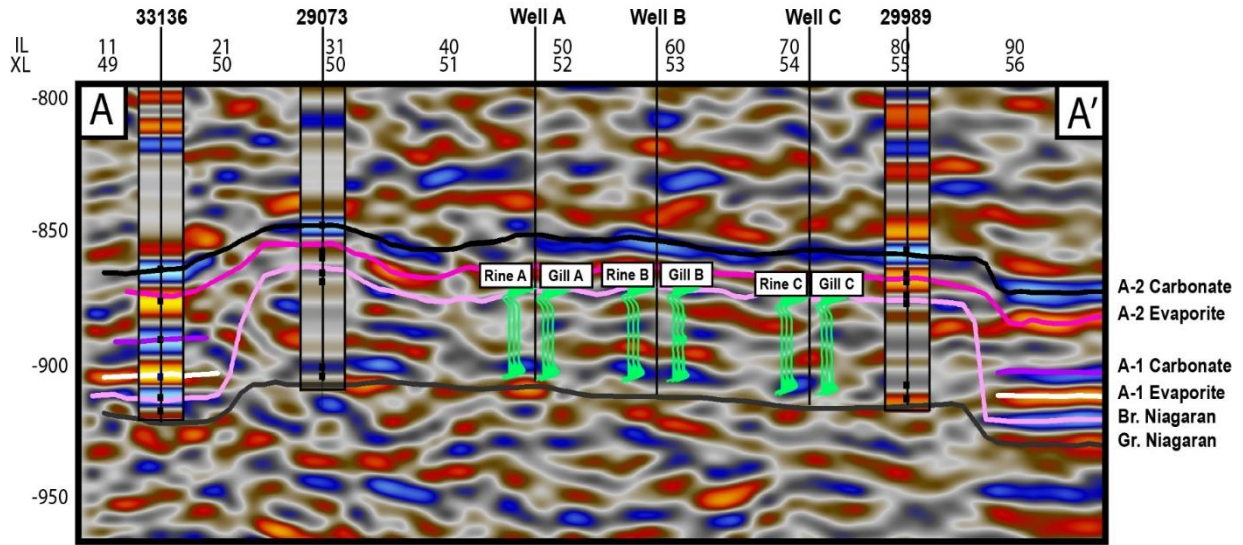
Figure 25. SW-NE cross-section through the seismic data with the pseudo synthetic seismograms overlaid on the seismic data. (Refer to previous figures for abbreviations)
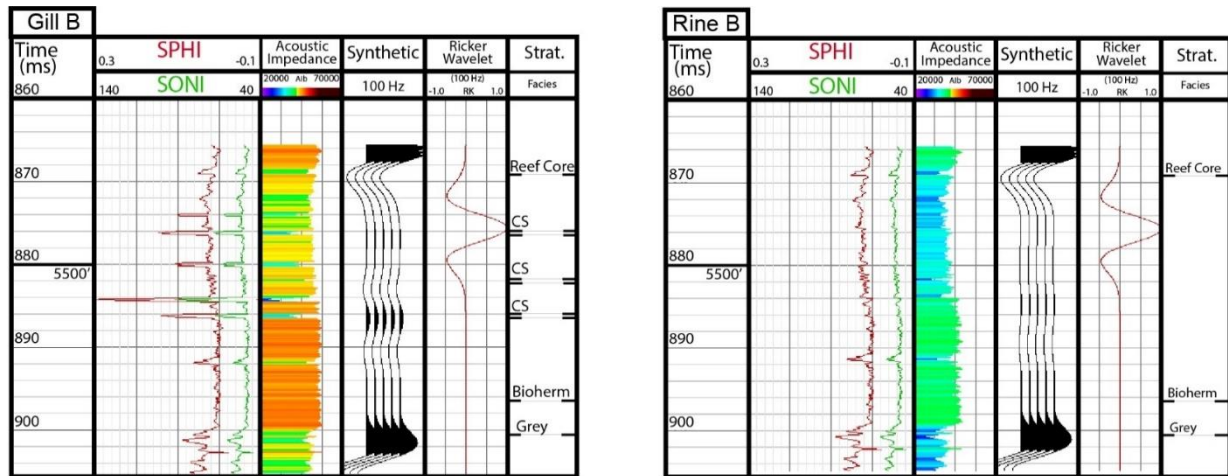
Figure 26. The two pseudo synthetic seismograms generated for pseudo Well B. (SPHI: Sonic Porosity, Strat.: Stratigraphy, CS: Coarse skeletal, Remaining abbreviations refer to previous figures)

CORE PHOTOS

PLATE 1
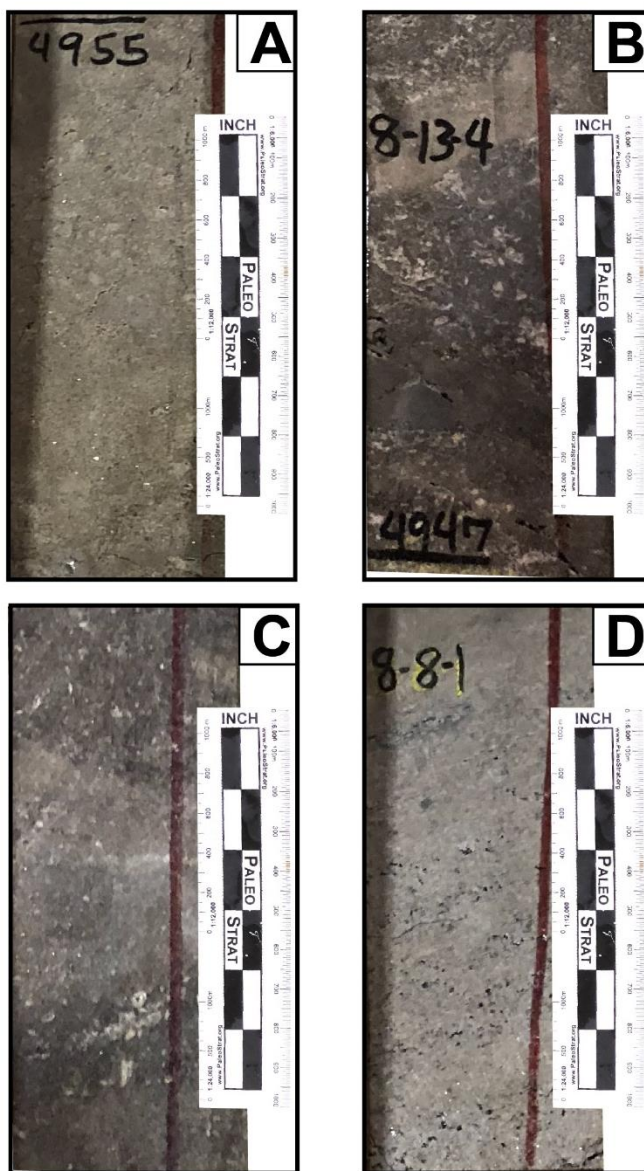
Plate 1-A: Core Depth – 4955' – Crystalline dolomite – Bioherm

Plate 1-B: Core Depth – 4947' – Mottled grey-white dolomite – Bioherm

Plate 1-C: Core Depth – 4939' – Mottled dolomite w/ crinoids – Bioherm

Plate 1-D: Core Depth – 4926' – Crystalline dolomite, no fossils – Bioherm Cap

PLATE 2
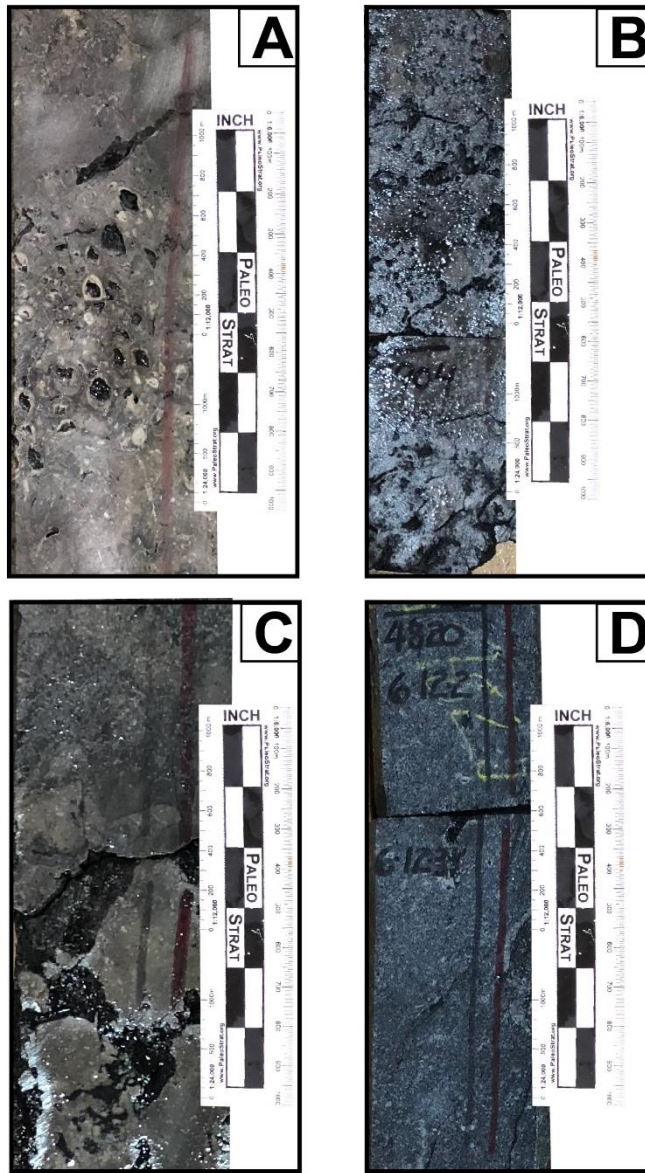
Plate 2-A: Core Depth – 4911' – Brachiopod skeletal wackestone – Reef Core

Plate 2-B: Core Depth – 4904' – Vuggy and fracture porosity – Reef Core

Plate 2-C: Core Depth – 4890' – Large vugs infilled w/organic matter – Reef Core

Plate 2-D: Core Depth – 4820' – Fractures infilled with calcite – Reef Core

PLATE 3
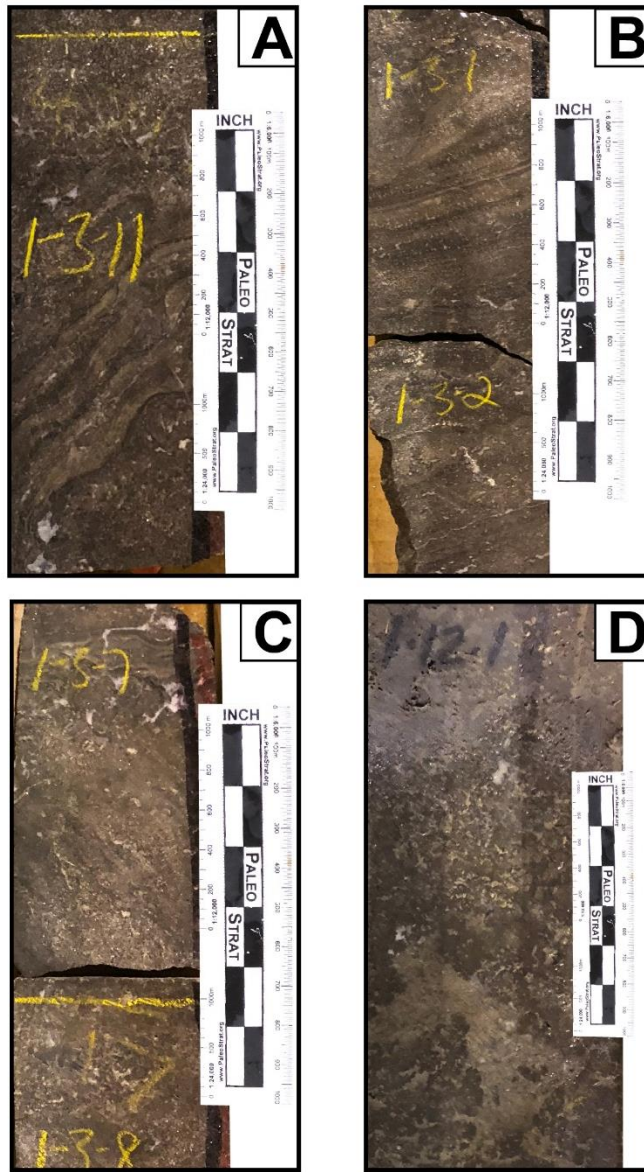
Plate 3-A: Core Depth – 4718' – High angle stromatolitic bindstone – Cyanobacterial Mats

Plate 3-B: Core Depth – 4715' – In-situ stromatolitic texture – Cyanobacterial Mats

Plate 3-C: Core Depth – 4717' – Stromatolitic conglomerate, calcite infilling – Cyanobacterial Mats

Plate 3-D: Core Depth – 4701' – Patchy/clotted thrombolitic texture – Thrombolitic Bindstone

PLATE 4
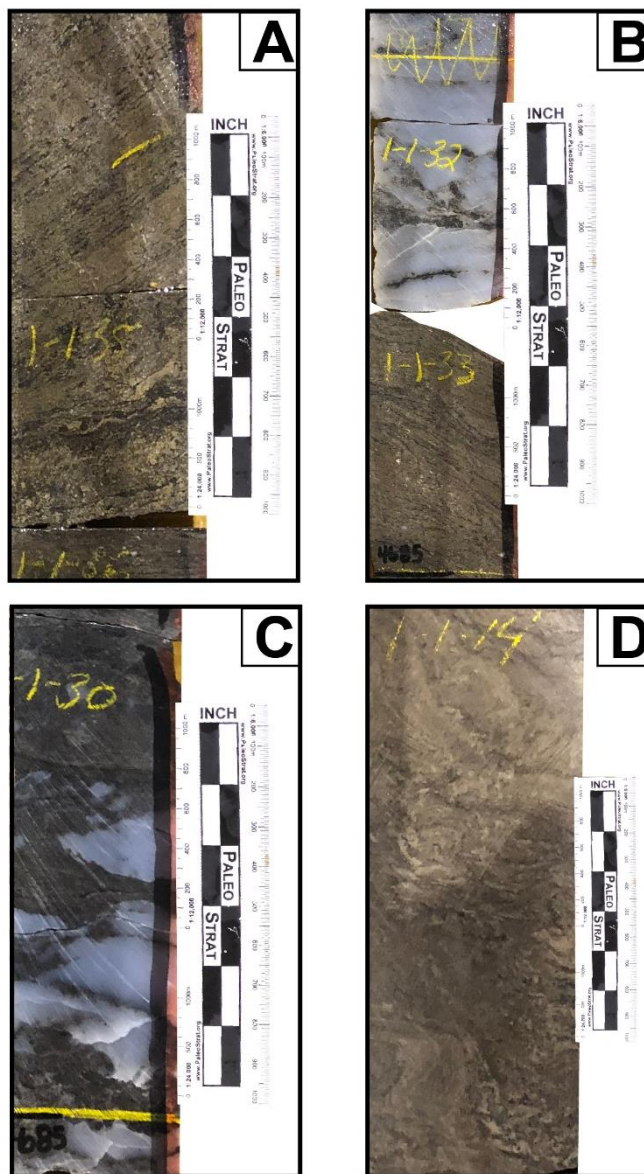
Plate 4-A: Core Depth – 4687' – slightly angled, non-crinkly laminations – Laminated Peloidal Wackestone

Plate 4-B: Core Depth – 4685.5' – sharp contact between laminations & anhydrite – Wackestone/REA contact

Plate 4-C: Core Depth – 4684.5' – Chicken-wire anhydrite nodules in dolomite matrix – Rabbit Ears Anhydrite

Plate 4-D: Core Depth – 4676' – wavy laminations w/ small anhydrite laths – A-1 Carbonate

REFERENCES CITED

Bristol, H.M., 1974, Silurian Pinnacle Reefs and Related Oil Production in Southern Illinois: Illinois State Geological Survey Illinois Petroleum 102, 98 p.

Brown, A.R., 1996, Interpretation of Three-Dimensional Seismic Data: American Association of Petroleum Geologists Memoir 42, 4th ed., 424 p.

Bubb, J.N., and Hatlelid, W. G., 1978, Seismic Stratigraphy and Global Changes of Sea Level, Part 10: Seismic Recognition of Carbonate Buildups: The American Association of Petroleum Geologists Bulletin, v. 62, no. 5, p. 772-791.

Gardner, G. H., Gardner, L. W., and Gregory, A. R., 1974, Formation Velocity and Density-The Diagnostic Basic for Stratigraphic Traps: Society of Exploration Geophysicists: Geophysics, v. 39, no. 6, p. 770-780, doi:10.1190/1.1440465.

Gill, D., 1973, Stratigraphy, Facies, Evolution and Diagenesis of Productive Niagaran Guelph Reefs and Cayugan Sabkha Deposits, The Belle River Mills Gas Field, Michigan Basin [Ph.D. thesis]: Ann Arbor, University of Michigan, 275 p.

Grammer, M., Barnes, D., Harrison III, B., Sandomierski, A., and Mannes, R., 2008, Practical synergies for increasing domestic oil production and geological sequestration of anthropogenic CO2: An example from the Michigan Basin, *in* M. Grobe, J. C. Pashin, and R. L. Dodge, eds., Carbon dioxide sequestration in geological media – State of science: AAPG Studies 59, p. 1-18.

Huh, J., 1973, Geology and diagenesis of the Niagaran pinnacle reefs in the northern shelf of the Michigan Basin [Ph.D. thesis]: Ann Arbor, University of Michigan.

Khan, A. K., Gulraiz, A., Work flow shown to develop useful seismic velocity models: Oil & Gas Journal, v. 109, no. 36, Exploration and Development: Special Report: Applied Geophysics

Kleipool, L.M., Jong, K. D., Vaal, E. D., and Reijmer, J. J., 2017, Seismic characterization of switching platform geometries and dominant carbonate producers (Miocene, Las Negras, Spain): Journal of the International Association of Sedimentologists, v. 64, p. 1676-1707, doi:10.1111/sed.12369.

Mesolella, K. J., Robinson, J. D., McCormick, L. M. and Ormiston, A. R., 1974, Cyclic Deposition of Silurian Carbonates and Evaporites in Michigan Basin: The American Association of Petroleum Geologists Bulletin, v. 58, no. 1, p. 34-62

Rine, M. J., 2015, Depositional Facies and Sequence Stratigraphy of Niagaran-Lower Salina Reef Complex Reservoirs of the Guelph Formation, Michigan Basin [M.S. thesis]: Kalamazoo, Western Michigan University, 185 p.

Rine, M. J., Garrett, J. D., and Kaczmarek, S. E., 2017, A New Facies Architecture Model for the Silurian Niagaran Pinnacle Reef Complexes of the Michigan Basin: Kalamazoo, Western Michigan University, 17 p.

Sheriff, R.E., 1993, Vertical and lateral seismic resolution and attenuation, *in* Morton-Thompson, D., and Woods, A., eds., Methods in Exploration Series, no. 10: American Association of Petroleum Geologists, 548 p.

Strauss, P., Harzhauser, M., Hinsch, R., and Wagreich, M., 2006, Sequence stratigraphy in a classic pull-apart basin (Neogene, Vienna Basin). A 3D seismic based integrated approach: Geologica Carpathica, v. 57, no. 3, p. 185-197.

Toelle, B., Pekot, L., Barnes, D., Grammer, M., and Harrison, W, 2008, EOR Potential of the Michigan Silurian Reefs Using CO2. Society of Petroleum Engineers: Proceedings of the Society of Petroleum Engineers Improved Oil Recovery Symposium, Tulsa, Oklahoma, SPE 113843-PP, p. 1-8.

Toelle, B. E., 2012, Use of 3D Seismic Azimuthal Iso-Frequency Volumes for the Detection and Characterization of High Porosity/Permeability Zones in Carbonate Reservoirs [Ph.D. thesis]: Morgantown, West Virginia University, 186 p.

Victorine, J.R., 1999, Synthetic Seismic Profile Plot: A web application for constructing synthetic seismograms from well log data: Kansas Geological Survey, http://www.kgs.ku.edu/software/SS/

White, R., and Simm, R., 2003, Tutorial: Good practice in well ties: European Association of Geoscientists & Engineers: First Break, v. 21, p. 75-83